Atmos. Chem. Phys. Discuss., 13, 21455–21505, 2013
www.atmos-chem-phys-discuss.net/13/21455/2013/
doi:10.5194/acpd-13-21455-2013

Atmospheric Chemistry and Physics Discussions

Combined assimilation of IASI and MLS observations to constrain tropospheric and stratospheric ozone in a global chemical transport model

E. Emili[1], B. Barret[3], S. Massart[4], E. Le Flochmoen[3], A. Piacentini[1], L. El Amraoui[2], O. Pannekoucke[1,2], and D. Cariolle[1]

[1]CERFACS, Toulouse, France
[2]Météo France, Toulouse, France
[3]Laboratoire d'Aérologie, Toulouse, France
[4]ECMWF, Reading, UK

Received: 15 July 2013 – Accepted: 30 July 2013 – Published: 20 August 2013

Correspondence to: E. Emili (emili@cerfacs.fr)

Published by Copernicus Publications on behalf of the European Geosciences Union.

Abstract

Accurate and temporally resolved fields of free-troposphere ozone are of major importance to quantify the intercontinental transport of pollution and the ozone radiative forcing. In this study we examine the impact of assimilating ozone observations from the Microwave Limb Sounder (MLS) and the Infrared Atmospheric Sounding Interferometer (IASI) in a global chemical transport model (MOdèle de Chimie Atmosphérique à Grande Échelle, MOCAGE). The assimilation of the two instruments is performed by means of a variational algorithm (4-D-VAR) and allows to constrain stratospheric and tropospheric ozone simultaneously. The analysis is first computed for the months of August and November 2008 and validated against ozone-sondes measurements to verify the presence of observations and model biases. It is found that the IASI Tropospheric Ozone Column (TOC, 1000–225 hPa) should be bias-corrected prior to assimilation and MLS lowermost level (215 hPa) excluded from the analysis. Furthermore, a longer analysis of 6 months (July–August 2008) showed that the combined assimilation of MLS and IASI is able to globally reduce the uncertainty (Root Mean Square Error, RMSE) of the modeled ozone columns from 30 % to 15 % in the Upper-Troposphere/Lower-Stratosphere (UTLS, 70–225 hPa) and from 25 % to 20 % in the free troposphere. The positive effect of assimilating IASI tropospheric observations is very significant at low latitudes (30° S–30° N), whereas it is not demonstrated at higher latitudes. Results are confirmed by a comparison with additional ozone datasets like the Measurements of OZone and wAter vapour by aIrbus in-service airCraft (MOZAIC) data, the Ozone Monitoring Instrument (OMI) total ozone columns and several high-altitude surface measurements. Finally, the analysis is found to be little sensitive to the assimilation parameters and the model chemical scheme, due to the high frequency of satellite observations compared to the average life-time of free-troposphere/low-stratosphere ozone.

ACPD
13, 21455–21505, 2013

1 Introduction

Tropospheric ozone (O_3) is the third most important gas in its contribution to the global greenhouse effect after CO_2 and CH_4 (Solomon et al., 2007). It is also a major pollutant in the planetary boundary layer, with adverse effects on humans health (Brunekreef and Holgate, 2002) and plants (Avnery et al., 2011). Its production is mainly driven by emissions of primary pollutants such as nitrogen oxides (NO_x), carbon monoxide (CO) and Volatile Organic Compounds (VOCs), followed by photolysis and non-linear chemistry reactions. Since it has an average life-time of about two weeks, it can be efficiently transported for several thousands of km in the free troposphere (Zhang et al., 2008; Ambrose et al., 2011). Quantifying the impact of tropospheric ozone transport is especially important for those countries that, despite air-quality related regulations, experience a significant ozone background increase (Jaffe and Ray, 2007; Tanimoto, 2009). Moreover, intrusions of ozone-rich air from the stratosphere via stratosphere-troposphere exchanges (STE) are among the principal causes of high free-troposphere ozone episodes (Stohl et al., 2003; Barré et al., 2012). Therefore, a precise characterization of both low-stratosphere and tropospheric ozone is required to properly quantify ozone transport.

Ozone-sondes provide observations of tropospheric and stratospheric ozone with high vertical resolution (Komhyr et al., 1995), but their geographical distribution is sparse and they are not very frequent in time. Satellite observations of ozone are available since the early 70s (Fioletov et al., 2002) but they provided mainly stratospheric ozone profiles or total columns. Since the stratospheric ozone concentration is higher than the tropospheric one by several orders of magnitude, total column retrievals do not provide a strong sensitivity to tropospheric ozone. Several studies derived tropospheric ozone columns by means of subtracting the measured stratospheric amount from the total column (Ziemke et al., 2006; Kar et al., 2010; Yang et al., 2010). However, these techniques are limited by the difficulties that arise from combining data from instruments with different calibration and spatio-temporal resolutions (Ziemke et al., 2011).

ACPD
13, 21455–21505, 2013

The latest generation of thermal infrared spectrometers, onboard low-earth orbit (LEO) satellites, is able to capture the tropospheric ozone signature (Eremenko et al., 2008; Boynard et al., 2009; Barret et al., 2011; Tang and Prather, 2012). The Tropospheric Emission Spectrometer (TES) provides for example almost two pieces of independent information (degrees of freedom for signal, DFS) in the troposphere (Zhang et al., 2010) with a global coverage in 16 days. The Infrared Atmospheric Sounding Interferometer (IASI) allows a daily global coverage at very high spatial resolution (12 km for nadir observations), with a slightly reduced number of tropospheric DFS ($\sim$ 1, Dufour et al., 2012), although the DFS value might also be sensible to the choice of the tropopause height and the retrieval technique. In general, satellites data permit to catch major features of ozone tropospheric distribution (Ziemke et al., 2009; Hegarty et al., 2010; Barret et al., 2011) but observations frequency and data gaps (e.g. due to clouds) do not allow a complete view of the underlying dynamics at short time scales (e.g. hours).

Chemical transport models (CTM), through data assimilation (DA), can ingest information from satellite observations in a coherent way (e.g. by considering the vertical sensitivity of the instrument) and use them to update the modeled 3-D ozone field. Likewise, satellite retrievals themselves are normally based on the inversion of the measured radiance data with a variational approach, thus requiring an a-priori profile from a model or a climatology as ancillary input (Eskes and Boersma, 2003). Data assimilation of stratospheric ozone profiles, total columns or ozone sensitive radiances is nowadays well integrated in operational meteorological models (Jackson, 2007; Dee et al., 2011), which are generally based on simplified ozone chemistry schemes (Geer et al., 2007). Assimilation of satellite O_3 products has also been investigated in a number of studies with CTMs including comprehensive chemistry schemes (Geer et al., 2006; Lahoz et al., 2007b; van der A et al., 2010; Doughty et al., 2011). Furthermore, chemical data assimilation is becoming more and more part of operational services, as demonstrated by projects like the Monitoring Atmospheric Composition and Climate initiative (MACC, Inness et al., 2013).

ACPD
13, 21455–21505, 2013

Parrington et al. (2009) and Miyazaki et al. (2012) assimilated TES data to constrain tropospheric ozone, finding consistent improvements with regard to the respective model background field. However, few studies explored the assimilation of ozone data from IASI, which is the only sensor sensible to tropospheric ozone and with a global daily coverage (night and day). Massart et al. (2009) assimilated IASI total columns but did not use averaging kernel informations to separate tropospheric and stratospheric signal. Han and McNally (2010) assimilated IASI radiances in the ECMWF 4-D-VAR system and found a better fit of the analysis to ozone profiles from the Microwave Limb Sounder (MLS), but effects on tropospheric ozone were not discussed. Coman et al. (2012) assimilated 0–6 km ozone columns in a regional CTM and found improved ozone concentrations also at the surface. To our knowledge there is still no study that examined the assimilation of IASI tropospheric ozone columns globally. Moreover, the combined assimilation of generally accurate MLS profiles in the stratosphere (Massart et al., 2012) and IASI tropospheric columns is supposed to better constrain the ozone gradients at the tropopause and the ozone exchanges between the two layers. Finally, CTMs that use detailed chemistry schemes are numerically more expensive than those using simplified linear schemes for the ozone and require emission inventories, which can be quite uncertain in some regions of the world (Ma and van Aardenne, 2004). Since the spatial coverage of IASI observations is very high and the ozone average life-time is longer than the revisiting time of the satellite, we can expect that the degree of complexity of the CTM used for the assimilation might become less relevant. The objective of this study is to explore the potential of IASI and MLS Level 2 products to provide global analyses and forecasts of ozone, with a focus on the free-troposphere dynamics.

We assimilate ozone stratospheric profiles from MLS and tropospheric partial columns from IASI to constrain the global ozone concentration calculated with the MOdèle de Chimie Atmosphérique á Grande Échelle CTM (MOCAGE, Teyssèdre et al., 2007). The model can be used in combination with a linear ozone chemistry parametrization (Cariolle and Teyssedre, 2007) or with a detailed strato-

ACPD
13, 21455–21505, 2013

sphere/troposphere chemistry. In the first case, surface emissions are not considered and a relaxation term to a climatological field is dominant in the troposphere. With this configuration we computed ozone reanalysis for the period that goes from July 2008 to December 2008.

The paper is structured as follows: Sect. 2 describes the assimilated observations and those used for the validation, the model and the assimilation algorithm are detailed in Sect. 3, Sect. 4 contains the discussion of the different simulations and their validation. Finally, conclusions are given in Sect. 5.

2 Ozone observations

2.1 Assimilated observations

2.1.1 MLS profiles

The Microwave Limb Sounder (MLS) instrument has been flying onboard the Aura satellite in a sun-synchronous polar orbit since August 2004. It measures millimetre and sub-millimetre thermal emission at the atmospheric limb, providing vertical profiles of several atmospheric parameters (Waters et al., 2006). It allows the retrieval of about 3500 profiles per day with a nearly global latitude coverage between 82° S and 82° N. The version 2.2 of the MLS ozone product is used in this study. Since the along-track distance between two successive MLS profiles (1.5°) is smaller than the model horizontal resolution (2.0°) all the profiles measured within a minute are averaged and assigned to the same grid cell. This reduces the number of profiles to about 2000 per day. A data screening based on the recommendations of Froidevaux et al. (2008) and Livesey et al. (2008) is used, as in Massart et al. (2009, 2012). Therefore, the assimilated ozone profile consists of 16 pressure levels in the range from 215 to 0.5 hPa, with four of them located in the Upper-Troposphere/Lower-Stratosphere (UTLS). The MLS ozone profile accuracy is the lowest in the UTLS, with biases that can be as high

ACPD
13, 21455–21505, 2013

as 20 % at 215 hPa, whereas the precision is about 5 % elsewhere (Froidevaux et al., 2008). The MLS product provides a profile retrieval uncertainty based on error propagation estimations and information about the retrieval vertical sensitivity through the averaging kernels (AVK). The MLS O_3 product has been already assimilated in multiple models with positive effects on models' scores in the stratosphere (Jackson and Orsolini, 2008; Stajner et al., 2008; Massart et al., 2009; El Amraoui et al., 2010; Barré et al., 2012). Since the MLS AVK peaks sharply on the retrieved pressure layers, they can be neglected in the data assimilation procedure (Massart et al., 2012).

2.1.2 IASI partial columns

IASI-A is the first IASI thermal infrared interferometer launched in 2006 onboard the Metop-A platform (Clerbaux et al., 2009). It is a meteorological sensor dedicated to the measurement of tropospheric temperature, water vapour and of the tropospheric content of a number of trace gases. Thanks to its large swath of 2200 km, IASI enables an overpass over each location on the Earth surface twice daily. The Software for a Fast Retrieval of IASI Data (SOFRID) has been developed at Laboratoire d'Aérologie to retrieve O_3 and CO profiles from IASI radiances (Barret et al., 2011). The SOFRID is based on the Radiative Transfer for TOVS (RTTOV) code and on the 1-D-VAR retrieval scheme both developed for operational processing of space-borne data within the Numerical Weather Prediction – Satellite Application Facilities (NWP-SAF). For each IASI pixel, SOFRID retrieves the O_3 volume mixing ratio (vmr) on 43 pressure levels between 1000 and 0.1 hPa. Nevertheless, the number of independent pieces of information or Degrees of Freedom for Signal (DFS) of the retrieval is approximately 3 for the whole vertical profile (Dufour et al., 2012). Barret et al. (2011) have shown that IASI enables the independent determination of the Tropospheric O_3 Column (TOC, 1000–225 hPa) and the UTLS (225–70 hPa) O_3 column with DFS close to unity for both quantities over tropical regions. The information content analysis from Dufour et al. (2012) provides similar conclusions for both the mid-latitudes and the tropics with slightly different definitions of the tropospheric and UTLS partial columns. In order to be consistent

ACPD
13, 21455–21505, 2013

with these information content analyses and to improve the efficiency of our assimilation system, we assimilate IASI TOC instead of whole profiles. The IASI TOC was also validated against ozone-sondes and airborne observations in Barret et al. (2011). Accuracies of 13 ± 9 % (relative bias ± standard deviation) have been found at high latitudes and of 5 ± 15 % within the tropics. Therefore, a global bias correction of 10 % of SOFRID values is performed, its impact being carefully discussed further in the paper. In order to remove observations with little information, pixels with TOC DFS lower than 0.6 are also screened out.

2.2 Validation observations

2.2.1 Ozone-sondes profiles

Ozone-sondes are launched in many locations of the world on a weekly schedule (Fig. 1), measuring vertical profiles of ozone concentration with high vertical resolution (150–200 m) up to approximately 10 hPa. Data are collected by the World Ozone and Ultraviolet Radiation Data Centre (WOUDC, http://www.woudc.org/). Most of the sondes (85 %) are of Electrochemical Concentration Cell (ECC) type, the rest of them being of Carbon-Iodide or Brewer-Mast type. This introduces some heterogeneity in the measurement network. However, it has been shown that ECC sondes, which constitute the largest part of the network, have a precision of about 5 % regardless the calibration procedure employed (Thompson et al., 2003). Moreover, ozone-sondes data are here used to validate ozone numerical models, which introduce an additional representativity error, and such a precision is considered sufficient. Errors might increase to 10 % where ozone amounts are low (e.g. upper troposphere and upper stratosphere, Komhyr et al., 1995). To exploit the high vertical resolution of ozone-sondes data the profiles are log-normally interpolated on the coarser model grid (60 sigma-hybrid levels, Sect. 3.1). Information about the horizontal drift of sondes measurements is often not given and will not be considered in the study.

ACPD
13, 21455–21505, 2013

2.2.2 MOZAIC measurements

The Measurements of OZone and wAter vapour by aIrbus in-service airCraft (MOZAIC) program (Marenco et al., 1998) was initiated in the 90s with the aim to provide a global and accurate dataset for upper-troposphere chemistry and model validation. Automated instruments mounted on-board of several commercial airplanes measure ozone concentration every 4 s with a precision of about ±2 parts per billion by volume (ppbv) or ±2%. Almost 90 % of data is collected at the airplane cruise altitude (∼ 200 hPa) and the remaining 10 % during the takeoff/landing.

2.2.3 OMI total columns

The Ozone Monitoring Instrument (OMI), onboard Aura satellite, is a nadir viewing imaging spectrometer that measures the solar radiation reflected by the Earth's atmosphere and surface (Levelt et al., 2006). It makes spectral measurements in the ultraviolet/visible wavelength range at 0.5 nm resolution and with a very high horizontal spatial resolution (13 km × 24 km pixels). In the standard global observation mode, 60 across-track ground pixels are acquired simultaneously, covering an horizontal swath approximately 2600 km wide, which enables measurements with a daily global coverage. In this study, we use the OMI Level 3 globally gridded total ozone columns (OMDOAO3e.003) available at the GIOVANNI web portal (http://disc.sci.gsfc.nasa.gov/giovanni). This product is based on DOAS inversion (Veefkind et al., 2006). OMI DOAS total ozone columns agree within 2 % with ground-based observations (Balis et al., 2007), except for Southern Hemisphere (SH) high latitudes, where they are systematically overestimated by 3–5 %.

2.2.4 ESRL GMD in-situ measurements

The Earth System Research Laboratory (ESRL) Global Monitoring Division (GMD, http://www.esrl.noaa.gov/gmd/) maintains several US atmospheric composition obser-

ACPD
13, 21455–21505, 2013

vatories and collects data from a number of other institutions. Time series of hourly ozone concentration are available at 2 sites located above 3000 m altitude, Mauna Loa (MLO, 19.54° N, 155.58° W, 3397 m a.s.l., US) and Summit (SUM, 75.58° N, 38.48° W, 3216 m a.s.l., Greenland), thus representative for the free-troposphere. Since the mission of the GMD is to provide accurate long-term time series of atmospheric constituents for climate analysis, the calibration stability of these measurements is expected to be within 2 % and data quality is assured by manual inspection (Oltmans et al., 2006).

3 Model description

3.1 Direct model

MOCAGE (MOdèle de Chimie Atmosphérique á Grande Échelle) is a three-dimensional CTM developed at Météo France (Peuch et al., 1999) that calculates the evolution of the atmospheric composition in accordance with dynamical, physical and chemical processes. It provides a number of configurations with different domains and grid resolutions, as well as chemical and physical parametrization packages. It can simulate the planetary boundary layer, the free troposphere, the stratosphere and a part of the mesosphere. MOCAGE is currently used for several applications: e.g. the Météo-France operational chemical weather forecasts (Dufour et al., 2005), the Monitoring Atmospheric Composition and Climate (MACC) services (http://www.gmes-atmosphere.eu), studies about climate trends of atmospheric composition (Teyssèdre et al., 2007). It has also been validated using a large number of measurements during the Intercontinental Transport of Ozone and Precursors (ICARTT/ITOP) campaign (Bousserez et al., 2007). In this study, we used the 2° × 2° degrees global version of MOCAGE, with 60 sigma-hybrid vertical levels (from the surface up to 0.1 hPa). The transport of chemical species is based on a semi-lagrangian advection scheme (Josse et al., 2004) and depends upon ancillary meteorological fields. The meteorological

ACPD
13, 21455–21505, 2013

forcing fields used in our configuration are the analyses provided by the operational European Centre for Medium-Range Weather Forecasts (ECMWF) numerical weather prediction model. Among the different chemical schemes available within MOCAGE we selected for this study the linear ozone parametrization CARIOLLE.

The CARIOLLE scheme is based on the linearization of the ozone production/destruction rates with respect to ozone concentration, temperature and superjacent ozone column, which are precomputed using a 2-D (latitude-height) chemistry model (Cariolle and Teyssedre, 2007). Thus, it does not account for ozone production/destruction due to longitudinal and temporal variability of precursor species (e.g. NO_x), which limits the model accuracy especially in the planetary boundary layer. It includes an additional parametrization for the polar heterogeneous ozone chemistry, which allows the main features of stratospheric ozone depletion to be reproduced. It was shown that in the free troposphere and the stratosphere the linear parametrization has an accuracy similar to that of full chemical models (Geer et al., 2007). An analysis of the derivatives in the CARIOLLE scheme attests that ozone production/destruction rates are quite small below 20 km (< 1 ppbv h^{-1}), hence the transport plays the principal role in ozone dynamics at the time scales reckoned for satellite data assimilation (12–24 h). Since no tropospheric ozone removal process is modeled, a relaxation to an ozone climatology with an exponential folding time of 24 h is enabled in the lower troposphere, to avoid the excessive accumulation of ozone in the lowest layers during long simulations. The resulting relaxation rate (ppbv h^{-1}) is about 4 % of the difference between the climatological and the modeled profile, which is again negligible compared to the frequency of satellite assimilation increments.

3.2 Assimilation system

The data assimilation algorithm built around the MOCAGE model is named Valentina and was initially developed in the framework of the ASSET (Assimilation of Envisat data) project (Lahoz et al., 2007a). In its first implementation it was based on a 3-D-FGAT formulation (3-D-Variational in the First Guess at Appropriate Time variant,

ACPD
13, 21455–21505, 2013

Fisher and Andersson, 2001), which was used in numerous studies on continental or global scales, for the assimilation of satellite and in-situ O_3 and CO data (Massart et al., 2007, 2009; El Amraoui et al., 2008a, b, 2010; Claeyman et al., 2010; Barré et al., 2012; Jaumouillé et al., 2012).

In its latest version, a 4-D-VAR algorithm was implemented in Valentina (Massart et al., 2012). That allows the use of longer assimilation windows in the case of non-negligible ozone dynamics (e.g. due to strong transport) and a better exploitation of the spatio-temporal fingerprint of satellite observations (Massart et al., 2010). A 4-D-VAR algorithm requires a linear tangent of the forecast model and its adjoint, which can be numerically very costly for a complete chemistry scheme. These operators have been then developed only for the transport process and for the linear ozone chemistry scheme. Assimilation windows of 12 h have been used in this study. The Valentina observation operator (**H**) allows the assimilation of species concentration (e.g. vertical profiles or surface concentration), total and partial vertical columns, with the possibility to include averaging kernel information and multiple instruments at the same time. Since the model prognostic variables are the species concentration, it follows that **H** is also linear. The background error covariance matrix (**B**) formulation is based on the diffusion equation approach (Weaver and Courtier, 2001) and can be specified by means of a 3-D variance field (diagonal of **B**, in concentration units or as a % of the background field) and a 3-D field of correlation length scales. The observation error variance (e.g. the diagonal of **R**) can be assigned with explicit values (e.g. the pixel-based uncertainty included in some satellite products) or as % of the observation values. Only vertical error correlations are implemented in **R** in the case of profile type observations. The system provides the possibility for the adjustment of **B** and **R** diagonal terms, based on a-posteriori χ^2 statistics (Desroziers et al., 2005). For more details about the assimilation algorithm please refer to (Pannekoucke and Massart, 2008; Massart et al., 2009, 2012).

ACPD
13, 21455–21505, 2013

4 Results and discussion

Numerous assumptions about the statistics of the background and observation errors (**B** and **R** matrices) are required in data assimilation algorithms (Sect. 3.2). Besides, the paradigm that lies behind an optimal analysis demands that the model and the observations are unbiased with respect to the unknown truth. Nevertheless, biases may contribute significantly to the overall uncertainty of both models and observations. Several methods have been proposed to take into account model or observations biases (Dee and Uppala, 2009). However, no general strategy exists when both the model and the assimilated observations are biased, which is the case encountered in this study (as detailed in Sect. 2 for the observations and by Geer et al. (2007) for the model). Hence, the validation of the analysis against independent and accurate observations remains the only way to verify the correctness of prescribed **B** and **R** matrices.

In this study ozone-sondes data are used as reference to identify biases and estimate background error statistics. This approach requires that sondes profiles are unbiased and globally representative for the model, since the background error must be specified for the full model grid. Although their geographical distribution is not always homogeneous (e.g. in the Southern Hemisphere), WOUDC sondes are generally used to validate global models and satellite retrievals (Massart et al., 2009; Dufour et al., 2012).

Therefore, we proceed as follows: (i) we first run the model with/without DA for two months (August and November 2008); (ii) we compute global and monthly averages of model-sondes values for these two months to identify biases and estimate error statistics (Sects. 4.1, 4.2, 4.3.1); (iii) once the results are considered satisfactory, a longer simulation of 6 months (with/without DA) is performed and validated with additional datasets (Sect. 4.3.2).

The two months considered in (i) allow to test the analysis during different ozone regimes (e.g. the occurrence of South Pole ozone depletion in November). Moreover,

ACPD
13, 21455–21505, 2013

MLS and IASI analysis are first evaluated independently, to better understand the impact of the single instruments (Sects. 4.1 and 4.2), and coupled later on in Sect. 4.3.

Sondes data do not cover the upper stratosphere and assimilation parameters like error correlation length scales cannot be diagnosed using sondes sparse data. Thereafter, we also rely upon results from previous studies, which exploited ensemble methods to estimate the error statistics for the same model and observations used in this analysis (Massart et al., 2012). Eventually, sensitivity tests will be used to assure the robustness of the analysis to the variation of the assimilation parameters (Sect. 4.3.1).

Model simulations for August 2008 and November 2008, are initialized with the MLS analysis from the study of Massart et al. (2012). This analysis is considered as a testbed for assessing the additional benefits of IASI data assimilation. The 6 months-long simulation (Sect. 4.3.2) is instead initialized with 30 days of free model spin-up, as might be the case for an operational assimilation system, where previous analysis are not always available.

4.1 MLS profile assimilation

A MOCAGE-MLS ozone analysis for the entire year 2008 was examined in the study of Massart et al. (2012), with a focus on the stratosphere and on the effects of different background error parametrizations. In this section we repeat a similar analysis with particular attention to the tropopause region, which showed an enhanced bias in Massart et al. (2012) and is of greater interest for this study.

We computed the ozone field with a free run of the model (without DA, also named control run) in August/November 2008. The global average difference between this simulation and the ozone-sondes profiles is displayed in Fig. 1. Differences are presented in term of bias and Root Mean Square Error (RMSE) components and normalized with an ozone climatological profile (Paul et al., 1998). The number and the geographical position of sondes profiles used to calculate the error statistics are also shown. A total of 182 and 167 profiles are globally available for August and November respectively, with a greater representation in the Northern Hemisphere. The error curves show that

ACPD
13, 21455–21505, 2013

the model free run has globally a small relative bias (< 10%) except in November, inside the Planetary Boundary Layer (PBL, $p > 750$ hPa). The good free model performances are partly due to the accurate initial conditions prescribed on the first day of each month, which come from the previous MLS analysis. The relatively long life-time of ozone (Sect. 3.1) implies that, assuming a good description of the transport, the model error keeps memory of those conditions for several weeks. The RMSE profile in Fig. 1 shows that below 100 hPa the model total error increases up to about 30 %, with two higher peaks, one below the tropopause (~ 300 hPa) and the other in the PBL. Since the bias does not have such a distinct shape most of the RMSE error originates from the deficiencies of the model in reproducing the variability of measured ozone in these two layers. This behavior is not surprising in the troposphere, and especially in the PBL, since detailed ozone tropospheric chemistry is not taken into account within the O_3 linearized chemistry scheme. Moreover, since the initial condition comes from MLS analysis, the model was not constrained by any observation in the troposphere. We remark also that there is no evidence of a strong monthly dependence of the error profiles.

The parameter configuration used for the assimilation experiments presented in this and in the following sections is summarized in Table 1. Compared to the study of Massart et al. (2012), the background error variance is given in percentage of the ozone field (Fig. 2) and the vertical correlation length is set to one vertical grid point. Since the effects of using an ensemble based variance were not found to be highly significant and no estimation was available in the troposphere from the cited study, this choice was made to have a time dependent background error variance across the whole atmosphere. On the basis of the model free run validation (Fig. 1), we set a bigger uncertainty in the troposphere (30 %) than in the stratosphere (5 %). The choice of a small vertical correlation length arises from the fact that IASI's averaging kernels already spread its information vertically and we do not want the contribution from the two instruments to superpose too much in a first instance. We also simplified the horizontal correlation lengths diagnosed with the ensemble of MLS perturbed analysis in Massart

ACPD
13, 21455–21505, 2013

et al. (2012) with a zonal and time-independent average for the zonal length scale Lx (Fig. 2) and a constant value of 300 km for the meridional length scale Ly. All these simplifications are not supposed to influence greatly the analysis, given the results in Massart et al. (2012).

The validation of the MLS analysis is also shown in Fig. 1. When all MLS levels are used (Sect. 2) both the bias and the RMSE are reduced in the stratosphere ($p < 100$ hPa) but enhanced at around 300 hPa. This local degradation of the analysis was already observed in previous MLS assimilation studies (Stajner et al., 2008; Massart et al., 2012). Since there is strong evidence of a positive bias for the lowermost MLS level (215 hPa) (Jackson, 2007; Froidevaux et al., 2008), this level was removed from the assimilated dataset, leading to a better analysis (red line in Fig. 1). The stratospheric RMSE is globally reduced to almost 10 % both in August and November 2008. These results confirm the findings of a number of already cited studies that assimilated MLS ozone with other models. Note that, even after the exclusion of the 215 hPa MLS level, the analysis ozone profile between 200 hPa and 300 hPa still differs slightly from the control run. Since the vertical error correlation was fixed to 1 grid point and there is approximately a 8 grid points separation between the lowermost assimilated level (140 hPa) and the aforementioned layer, those changes are imputable to the model dynamics, likely through downward ozone transport (STE).

4.2 IASI TOC column assimilation

IASI retrieved ozone, unlike MLS ozone, has not been used in many assimilation studies. Therefore, a comparison between observations and the correspondent free model values allows a preliminary quantification of the scatter and the systematic biases between the two. Later, the validation of the assimilated fields with independent data will provide further insights about biases with respect to "true" ozone values.

Statistics of the differences between IASI observations and the free model ozone field are reported in Figs. 3 and 4, for August and November 2008, respectively. The IASI values used to compute these figures have been arbitrarily reduced by 10 %, to

ACPD
13, 21455–21505, 2013

compensate known retrieval biases (Sect. 2). The impact of such a bias correction on the further assimilation is detailed later in this section. IASI tropospheric partial columns (TOC, 225–1000 hPa) are compared to the free model equivalent columns by means of the observation operator, thus taking into account the spatio-temporal colocation and the satellite averaging kernels. Maps show that in both seasons the model significantly underestimates IASI partial columns at low latitudes (30° S–30° N) in the Middle East, Africa and Central/South America (bias as high as 10 DU, corresponding to ∼ 100% of model values). A smaller but positive bias (2–4 DU) is found at lower latitudes (30° S–90° S), which is however less significant compared to the greater local column amount. Average standard deviations are 2 DU (Dobson Units) for both seasons with maximum values of about 5 DU localized between 30° S–60° S and over desert regions (Saharan and Australian deserts).

High systematic differences are found in regions dominated by dust aerosols, like the Atlantic ocean band east of the Saharan desert (Remer et al., 2008). Dust aerosols are known to reduce the accuracy of infrared ozone retrievals, like IASI ones. However, IASI retrievals biases for the ozone total columns are normally lower than 30 % in presence of dust (Boynard et al., 2009) so that this cannot entirely explain the observed differences (as high as 100 %). Therefore the remaining systematic differences are mostly attributed to the model deficiencies. Indeed, the model underestimates ozone in several regions affected by biomass burning outflow, like eastern Africa in August, western South America in November or in the western Indian Ocean (van der Werf et al., 2006; Barret et al., 2011). The reason for such biases is the model simplified tropospheric chemistry, which does not take into account emissions of ozone precursors and their impact on local ozone chemistry. This will be confirmed by the independent validation carried further in this section.

The number of monthly observations in Figs. 3 and 4 shows that IASI data enable almost a 100 % coverage over oceans and, over land, more observations during the summer months than in the winter ones (August in the Northern Hemisphere and viceversa in the southern one). This is due to the stronger thermal contrast between

ACPD
13, 21455–21505, 2013

the atmospheric layers and the continental surface in summer, which enhances the DFS and the number of pixels that pass the AVK trace filter (Sect. 2). This is also the reason why the zonal averaging kernels (Figs. 3f and 4f), which depend mostly on the ocean–atmosphere thermal gradient, have a stronger peak during winter. Note that the low trace screening filters out most of the observations over ice and high altitude surfaces (e.g. Greenland, South Pole, Himalaya and Rocky mountains), which have a poor thermal contrast or not enough tropospheric pressure levels available. Finally, desert regions show also a decreased number of observations due to issues in correctly representing the sand emissivity in the infrared ozone retrieval.

Figure 5 shows the error profiles for the IASI TOC analysis. The initial condition and the assimilation configuration are the same as in the MLS analysis (Sect. 4.1 and Table 1) but no MLS data are assimilated at this point. Using horizontal length scales previously diagnosed with MLS ensembles (Fig. 2) might not be pertinent for the troposphere. Nevertheless, IASI data coverage is very dense in space and time (Figs. 3 and 4) and the impact of the background error horizontal correlations is supposed to be exiguous. This will also be illustrated later in the article (Sect. 4.3.1).

When IASI data are not bias-corrected the analysis is sometimes worse than the control run (Fig. 5): the tropospheric bias increases by 10–20 % for both months and the RMSE improves in August but deteriorates in November. Instead, when 10 % of the values is globally removed from IASI observations the bias of the analysis improves or stays the same with respect to the control run and the RMSE is reduced by about 5–10 % in both months. The profile is corrected significantly only between 200 hPa and 800 hPa, where the AVK values are greater than 10 DU vmr^{-1} (Figs. 3 and 4). Comparing the curves in Figs. 1 and 5 we conclude that with the selected value of the background error vertical correlation, the correction brought by the two instruments (MLS and IASI) remains well separated vertically.

Compared with previous attempts of assimilating IASI total ozone columns in a CTM (Massart et al., 2009), we found a clear improvement in the tropospheric ozone profile. The main reason is attributed to the the full exploitation of the IASI tropospheric

ACPD
13, 21455–21505, 2013

signal in this study. Neglecting the AVK information lead to significantly worse results (not shown), which demonstrates their importance in the vertical localization of the assimilation increments. Several assimilation experiments were done with a different definition of the TOC column, obtained by lowering the top height of the column to 300, 400 and 500 hPa. Since the AVK is spread above the specified column top height, this was done to reduce the possible contamination of stratospheric air masses at high latitudes, which might introduce positive tropospheric ozone biases in the analysis. No significant improvements were however observed in any of these analyses.

4.3 MLS + IASI combined assimilation

In the previous sections MLS and IASI ozone products have been assimilated separately during August and November 2008. The purpose was to test the assimilation algorithm and detect issues like observational biases, with the help of sondes data. In this section the combined assimilation of both instruments is detailed: still for the two months separately first, and for a simulation of 6 months (July–December 2008) later. In addition to the usual validation against sondes data, a comparison with OMI total ozone columns and free troposphere in-situ measurements are reported. This will better clarify the added value of the IASI assimilation compared to the MLS on its own.

Figure 6 depicts the error profiles (bias and RMSE) of the combined analysis for August and November 2008 and the zonal differences between the analysis and the control run. Since the increments due to the two instruments are quite separated vertically, the error profile of the combined analysis is almost equivalent to the combination of the error profiles of the two separated analyses (Figs. 1 and 5). The zonal differences (Fig. 6c and f) show that the ozone concentration is increased by 20–30 % in the tropical region (30° S–30° N) both in the troposphere and in the lower stratosphere, and decreased by 10–20 % in the southern latitudes (30° S–90° S) free troposphere and at about 10 hPa. The patterns are similar in August and November, except for the northern latitudes (60° N–90° N) troposphere and the tropical stratosphere (in the vicinity of 10 hPa), where the differences change sign among the two months. Moreover, the

ACPD
13, 21455–21505, 2013

tropospheric positive increment is slightly shifted toward the northern mid-latitudes in summer (40° N). The average increments are able to correct most of the deficiencies of the direct model, which are: (i) the lack of ozone precursors emissions and chemistry in the tropical/mid-latitudes troposphere and (ii) the presence of high-latitude stratospheric positive biases due to a too strong polar-ward circulation in the forcing wind field (Cariolle and Teyssedre, 2007; de Laat et al., 2007).

A complementary validation of the ozone fields obtained with the combined assimilation is provided by a comparison with MOZAIC data. These data allow a good geographical and temporal coverage in the Northern Hemisphere, due to the daily frequency of commercial flights, but with 90 % of the data vertically confined at the airplane cruise altitude (~ 200 hPa). Scatter plots between model ozone values and MOZAIC observations above 400 hPa are reported in Fig. 7. Raw data were temporally averaged on a minute basis to better fit the model spatial resolution. Some data redundancy might still be present, even though the validation statistics are not supposed to be sensitive to that. Overall the relative error lies between 35 and 40 %. The scores are very similar to those obtained using sondes data (Fig. 6, 200 hPa level) and highlight a modest improvement of the correlation and the RMSE for the IASI-MLS analysis in August and a slight worsening in November. Therefore we only consider sondes data hereafter.

Figure 8 shows the geographical differences of the TOC among the control run and the analysis. In addition to Fig. 6, which already highlighted the zonal features of the increments, we note a significant increase of the TOC over the African continent and the Atlantic region, whereas the local ozone minimum over Indonesia is not changed or even slightly decreased. This is consistent with the preliminary comparison between modeled and IASI ozone shown in Figs. 3 and 4. The main spatial features of the analysis in the tropics are well comparable with the satellite climatology of TOC ozone derived by Ziemke et al. (2011). Differences between the two datasets depend not only on the methodology and the measurements being used, but also on the definition of the TOC column (1000–225 hPa in this study, surface-dynamical tropopause in Ziemke

ACPD
13, 21455–21505, 2013

et al., 2011). Hence, a more quantitative comparison would require the same definition of the TOC column to be adopted.

A quantitative comparison of the analysis with OMI total ozone columns is presented in Fig. 9. The comparison is done between independent averages of both datasets, which do not consider the exact temporal matching. Since OMI permits a daily global coverage, differences due to this reason are assumed negligible. The greatest positive correction originates from the assimilation of MLS data, which modify the more abundant stratospheric ozone. However, the addition of IASI TOC permits to reach the best agreement between the analysis and OMI data in the tropics, where the stratospheric column amount is lower and the total ozone column is more sensible to the tropospheric amount.

4.3.1 Sensitivity of the analysis to the background/observation error covariance

Before calculating the 6 months-long analysis, alternative formulations of the background and the observation error covariance matrices have been tested to verify the robus tness of the analysis to the choice of the assimilation parameters. The following cases have been considered, where the non-specified parameters are kept the same as in Table 1:

- temporally constant background variance expressed in ozone concentration units and derived from the MLS ensemble (Massart et al., 2012) above the tropopause (full 3-D field) and from sondes validation in the troposphere (zonally averaged field, three latitude bands used);
- background variance equal to 20 % of the ozone field everywhere, constant and homogenous horizontal error length scale equal to 4°;
- error statistics as in Table 1 but optimization of **B** and **R** matrix based on a-posteriori diagnostics (Sect. 3.2).

ACPD
13, 21455–21505, 2013

The first two represent two cases of more/less detailed **B** matrix and the last one a case of statistical optimization of **B** and **R** at the same time. In all cases the comparison with sondes profiles was not found to be superior or differences with the reference analysis were not significant (not shown). The reasons are attributed to the combination of the high temporal frequency of the assimilated satellite observations and the relatively slow ozone chemistry, which makes the background error strongly dependent on the initial condition. Once the model is corrected for the inexact initial conditions, further assimilation increments only bring minor adjustments, which keep the model close to the temporal trajectory of observations. This can be better clarified looking at the Observation minus Forecast (OmF) global statistics during the initial period of data assimilation in the case of the long run experiment (Fig. 10). The initial condition is not issued from a previous MLS analysis in this case but comes from a 30 days model spin-up period. It follows that, compared to the case of the simulations for August and November 2008, the model field differs initially more from the observations, especially the MLS ones. It takes approximately 3 days (6 assimilation windows) to reach the forecast-model minimum for both the OmF average and standard deviation. The model forecast at 10 hPa, which is initially biased high by 1000 ppbv and has a standard deviation of 400 ppbv with respect to MLS measurements, reduces its bias to 100 ppbv and its scatter to 200 ppbv after 4 assimilation windows (48 h). In the case of IASI the bias and the scatter are reduced just after 24 h to ~ 0 DU for the bias and 1.5–2 DU for the standard deviation from an initial value of 2 DU and 3 DU respectively. Subsequent values of OmF are of the order of the prescribed observation errors, which are about 200–300 ppbv for MLS 10 hPa level (Froidevaux et al., 2008) or 15 % of IASI TOC columns (Fig. 3), so that a further reduction is not possible. Note that IASI observations cover 80 % of the horizontal grid after 48 h, whereas MLS attains 40 % after 72 h (Fig. 10c). This explains the faster convergence of IASI OmF statistics. In other words, observations are dense enough to well constrain the long term (> 5 days) temporal evolution of the model, regardless of significant variations of the background covariance ma-

ACPD
13, 21455–21505, 2013

trix. Different choices of the background covariance may determine the rapidity of the convergence during the initial assimilation windows.

4.3.2 Validation of the 6 months-long simulations

The 6 months-long assimilation experiment (analysis) is initialized with a free model spin-up of 1 month in June 2008. The assimilation starts on 1 July 2008 and ends on 31 December 2008. For the same period a simulation without data assimilation (control run) is calculated.

Figure 11 shows the Taylor diagram of the collocated model-sondes columns. The 6 months period allows to accumulate enough sondes profiles to validate the model separately for different latitude bands. In addition to the TOC (1000–225 hPa), also the Upper Troposphere/Lower Stratosphere (UTLS, 225–70 hPa) column is considered. This type of plot depicts the capacity of the model to explain the variability of the validation dataset. In Figs. 12 and 13 columns/profiles bias, RMSE and standard deviation are also displayed to give a complete picture of the model performances. The results can be summarized as follows:

- Globally the UTLS column scores are significantly better for the analysis (R = 0.98, bias < 1 %, RMSE ~ 15 %) than for the control run (R = 0.9, bias ~ 15 %, RMSE ~ 30 %);
- The control run shows in particular a very high UTLS error in the 90° S–60° S band (bias ~ 50 %, RMSE ~ 60 %), due to the linear chemistry limitations with regards to the mechanism of ozone depletion;
- The TOC scores are also globally better for the analysis (R = 0.7, bias < 5 %, RMSE ~ 20 %) than for the control run (R = 0.6, bias ~ -10 %, RMSE ~ 25 %), even though to a lesser extent than in the case of the UTLS layer;

ACPD
13, 21455–21505, 2013

- All analysis TOC scores are significantly better than those of the control run at the tropics, but only the bias is substantially improved at northern mid-latitudes (from −15% to < 5%);
- In the 30° S–60° S and 60° N–90° N bands the TOC bias of the analysis field increases with respect to the control run. It follows that the analysis RMSE are not improved and the Taylor diagram scores are unchanged or even deteriorated;
- The analysis TOC is particularly inaccurate in the 90° S–60° S band ($R = 0.3$, bias ∼ 20 %, RMSE ∼ 25 %). However, the control run has already poor skills and very few IASI observations are assimilated during the whole period (Figs. 3 and 4).

The good quality of the UTLS ozone analysis with MLS data confirm the findings of previous studies (Jackson, 2007; El Amraoui et al., 2010; Massart et al., 2012). The results appear more heterogeneous with regards to the TOC analysis. The MLS-IASI assimilation has a robust and positive impact at low latitudes (30° S–30° N) which, however, becomes less evident at high latitudes and in polar regions. Other studies also identified difficulties in improving modeled tropospheric column at high latitudes by means of satellite data assimilation (Lamarque et al., 2002; Stajner et al., 2008). We conclude that IASI measurements, even if directly sensible to the tropospheric ozone concentration, are not able to fill this gap. Since modeled TOC at high latitudes is quite accurate (RMSE∼ 20%, Fig. 12), we assume that IASI retrieval biases become too large compared to model errors. Besides, the 10 % bias removed globally from IASI columns could have a zonal dependence, which was not considered in this study. However, additional validation studies of IASI products would be required to precisely assess this dependency.

Sondes data provide accurate information about the ozone vertical profile but their measurement frequency does not allow a daily- or hourly-scale validation of model predictions. Therefore, hourly measurements from two in-situ stations located above 3000 m are used to verify the free-troposphere ozone dynamics of the models. The two

ACPD
13, 21455–21505, 2013

selected sites are at the tropics (Mauna Loa, 19.54° N, 155.58° W) and at high latitudes (Summit, 75.58° N, 38.48° W). Figure 14 shows the time series of the analysis, the control run and the correspondent observations in August and November 2008. Since the ozone variability at very small spatial and temporal scales cannot be captured by a 2° × 2° grid model, original hourly observations have been smoothed in time using a moving average of ±6 h.

The control run underestimates the temporal variability of observations, as expected from a model that does not account for tropospheric chemistry. The analysis field has an increased variability when compared to the control one, still maintaining its low bias. However, the scores in term of correlation and standard deviation between the analysis time series and the observations (not shown) are not necessarily better than those of the control run. Note that at the Summit site and during August, the analysis is almost coincident with the control run because there are very few observations being assimilated in the surroundings (Fig. 3c).

This comparison leads to the conclusion that the assimilation of column integrated information corrects well the model TOC (e.g. at the tropics, Figs. 12 and 11) but does not necessarily improve the model prediction at a single vertical level. IASI AVK redistribute the satellite information in accordance with their vertical sensitivity and their a-priori, but the increments inside the partial column are still assigned proportionally to the model background profile. Hence, model predictions at a single vertical level do not necessarily ensure the same accuracy as the one found for partial columns.

5 Conclusions

In this study we examined the impact of MLS and IASI (SOFRID product) ozone measurements to constrain the ozone field of a global CTM (MOCAGE) by means of variational data assimilation and with particular emphasis on tropospheric ozone. Given the ozone average life-time of several weeks in the free troposphere, the high spatial cov-

ACPD
13, 21455–21505, 2013

erage of IASI data is expected to make up for the deficiencies of the linear chemistry model used.

Results confirm the effectiveness of MLS profiles assimilation in the stratosphere, with an average reduction of RMSE with respect to ozone-sondes from 30 % (model free run) to 15 % (analysis) for the UTLS column. The lowermost level of MLS data (215 hPa) was found to increase the analysis bias in the troposphere and is not further used. Improvements of the tropospheric columns (TOC) due to IASI O_3 data assimilation depend on the latitude and highlight the need to properly account for retrieval biases. When a globally constant 10 % positive bias is removed from IASI observations, the TOC RMSE decreases from 40 % (model free run) to 20 % (analysis) in the tropics and from 22 % to 17 % in the Northern Hemisphere (30° N–60° N) whereas it slightly increases (1–2 %) at other latitudes, probably due to residual IASI biases. Overall, the combined assimilation of MLS and IASI improves the correlations with ozone-sondes data for both the UTLS and TOC columns at almost all latitudes and increases the agreement with OMI total ozone column measurements. It is also found that the analysis is not very sensible to the parametrization of the background error covariance, due to the high temporal frequency of IASI and MLS observations and the strong dependency of the ozone field on the initial condition. Finally a comparison with hourly-resolved in-situ measurements in the free troposphere shows that assimilating information with a coarse vertical resolution increases the model variability but does not ensure a better hourly analysis at a particular vertical level.

We conclude that the assimilation of IASI and MLS data is very beneficial in combination with a linear ozone chemistry scheme. The high frequency of IASI observations is able to make up for model simplified tropospheric chemistry, especially at low latitudes and also in regions affected by strong seasonal emissions of ozone precursors (e.g. biomass burnings). Such an assimilation strategy provides reliable tropospheric and stratospheric ozone fields and might be valuable for a near-real time operational services and as benchmark for more sophisticated CTMs. Limitations concern surface ozone, where IASI low sensitivity cannot directly make up for missing ozone precur-

ACPD
13, 21455–21505, 2013

sors emissions and chemistry. However, IASI assimilation remains effective when the focus is on free-troposphere. Future applications of this system are the evaluation of tropopause ozone flux, a multi-annual climatology of global tropospheric ozone, analysis of major pollution episodes and prescription of chemical boundary conditions for regional models. Possible improvements of the IASI analysis might be obtained by assimilating IASI radiances directly into the CTM, thus considering a dynamical a-priori profile in the radiance inversion, instead of one issued from a climatology. Moreover, the development of a 4-D-VAR assimilation chain for the complete chemistry model will allow in future to consider the feedbacks of satellite ozone assimilation on other species.

Acknowledgements. This work was supported by the MACC, MACCII projects (funded by the European Commission under the EU Seventh Research Framework Programme, contract number 218793), the ADOMOCA project (funded by the French LEFE INSU program) and the TOSCA program (funded by the French CNES aerospace agency). We thank NASA for providing MLS and OMI satellite ozone products. OMI analyses used in this paper were produced with the Giovanni online data system, developed and maintained by the NASA GES DISC. We acknowledge the Ether French atmospheric database (http://ether.ipsl.jussieu.fr) for providing IASI data and the NOAA ESRL Global Monitoring Division (http://esrl.noaa.gov/gmd) for providing surface ozone measurements. We acknowledge for the strong support of the European Commission, Airbus, and the Airlines (Austrian-Airlines, Austrian, Air France) who carry free of charge the MOZAIC equipment and perform the maintenance since 1994. MOZAIC is presently funded by INSU-CNRS, Meteo-France, and FZJ (Forschungszentrum Julich, Germany). We thank all the individual agencies that provided ozone-sondes data through the World Ozone and Ultraviolet Radiation Data Centre (WOUDC).

References

Ambrose, J., Reidmiller, D., and Jaffe, D.: Causes of high O_3 in the lower free troposphere over the Pacific Northwest as observed at the Mt. Bachelor Observatory, Atmos. Environ., 45, 5302–5315, doi:10.1016/j.atmosenv.2011.06.056, 2011. 21457

ACPD
13, 21455–21505, 2013

Avnery, S., Mauzerall, D. L., Liu, J., and Horowitz, L. W.: Global crop yield reductions due to surface ozone exposure: 2. Year 2030 potential crop production losses and economic damage under two scenarios of O_3 pollution, Atmos. Environ., 45, 2297–2309, doi:10.1016/j.atmosenv.2011.01.002, 2011. 21457

Balis, D., Kroon, M., Koukouli, M. E., Brinksma, E. J., Labow, G., Veefkind, J. P., and McPeters, R. D.: Validation of Ozone Monitoring Instrument total ozone column measurements using Brewer and Dobson spectrophotometer ground-based observations, J. Geophys. Res.-Atmos., 112, D24S46, doi:10.1029/2007JD008796, 2007. 21463

Barré, J., Peuch, V.-H., Attié, J.-L., El Amraoui, L., Lahoz, W. A., Josse, B., Claeyman, M., and Nédélec, P.: Stratosphere-troposphere ozone exchange from high resolution MLS ozone analyses, Atmos. Chem. Phys., 12, 6129–6144, doi:10.5194/acp-12-6129-2012, 2012. 21457, 21461, 21466

Barret, B., Le Flochmoen, E., Sauvage, B., Pavelin, E., Matricardi, M., and Cammas, J. P.: The detection of post-monsoon tropospheric ozone variability over south Asia using IASI data, Atmos. Chem. Phys., 11, 9533–9548, doi:10.5194/acp-11-9533-2011, 2011. 21458, 21461, 21462, 21471

Bousserez, N., Attié, J. L., Peuch, V. H., Michou, M., Pfister, G., Edwards, D., Emmons, L., Mari, C., Barret, B., Arnold, S. R., Heckel, A., Richter, A., Schlager, H., Lewis, A., Avery, M., Sachse, G., Browell, E. V., and Hair, J. W.: Evaluation of the MOCAGE chemistry transport model during the ICARTT/ITOP experiment, J. Geophys. Res.-Atmos., 112, doi:10.1029/2006JD007595, 2007. 21464

Boynard, A., Clerbaux, C., Coheur, P.-F., Hurtmans, D., Turquety, S., George, M., Hadji-Lazaro, J., Keim, C., and Meyer-Arnek, J.: Measurements of total and tropospheric ozone from IASI: comparison with correlative satellite, ground-based and ozonesonde observations, Atmos. Chem. Phys., 9, 6255–6271, doi:10.5194/acp-9-6255-2009, 2009. 21458, 21471

Brunekreef, B. and Holgate, S. T.: Air pollution and health, Lancet, 360, 1233–42, doi:10.1016/S0140-6736(02)11274-8, 2002. 21457

Cariolle, D. and Teyssèdre, H.: A revised linear ozone photochemistry parameterization for use in transport and general circulation models: multi-annual simulations, Atmos. Chem. Phys., 7, 2183–2196, doi:10.5194/acp-7-2183-2007, 2007. 21459, 21465, 21474

Claeyman, M., Attié, J.-L., El Amraoui, L., Cariolle, D., Peuch, V.-H., Teyssèdre, H., Josse, B., Ricaud, P., Massart, S., Piacentini, A., Cammas, J.-P., Livesey, N. J., Pumphrey, H. C., and

ACPD
13, 21455–21505, 2013

Edwards, D. P.: A linear CO chemistry parameterization in a chemistry-transport model: evaluation and application to data assimilation, Atmos. Chem. Phys., 10, 6097–6115, doi:10.5194/acp-10-6097-2010, 2010. 21466

Clerbaux, C., Boynard, A., Clarisse, L., George, M., Hadji-Lazaro, J., Herbin, H., Hurtmans, D., Pommier, M., Razavi, A., Turquety, S., Wespes, C., and Coheur, P.-F.: Monitoring of atmospheric composition using the thermal infrared IASI/MetOp sounder, Atmos. Chem. Phys., 9, 6041–6054, doi:10.5194/acp-9-6041-2009, 2009. 21461

Coman, A., Foret, G., Beekmann, M., Eremenko, M., Dufour, G., Gaubert, B., Ung, A., Schmechtig, C., Flaud, J.-M., and Bergametti, G.: Assimilation of IASI partial tropospheric columns with an Ensemble Kalman Filter over Europe, Atmos. Chem. Phys., 12, 2513–2532, doi:10.5194/acp-12-2513-2012, 2012. 21459

de Laat, A. T. J., Landgraf, J., Aben, I., Hasekamp, O., and Bregman, B.: Validation of Global Ozone Monitoring Experiment ozone profiles and evaluation of stratospheric transport in a global chemistry transport model, J. Geophys. Res., 112, D05301, doi:10.1029/2005JD006789, 2007. 21474

Dee, D. P. and Uppala, S.: Variational bias correction of satellite radiance data in the ERA-Interim reanalysis, Q. J. Roy. Meteor. Soc., 1841, 1830–1841, doi:10.1002/qj.493, 2009. 21467

Dee, D. P., Uppala, S. M., Simmons, A. J., Berrisford, P., Poli, P., Kobayashi, S., Andrae, U., Balmaseda, M. A., Balsamo, G., Bauer, P., Bechtold, P., Beljaars, A. C. M., van de Berg, L., Bidlot, J., Bormann, N., Delsol, C., Dragani, R., Fuentes, M., Geer, A. J., Haimberger, L., Healy, S. B., Hersbach, H., Hólm, E. V., Isaksen, L., Kållberg, P., Köhler, M., Matricardi, M., McNally, A. P., Monge-Sanz, B. M., Morcrette, J.-J., Park, B.-K., Peubey, C., de Rosnay, P., Tavolato, C., Thépaut, J.-N., and Vitart, F.: The ERA-Interim reanalysis: configuration and performance of the data assimilation system, Q. J. Roy. Meteor. Soc., 137, 553–597, doi:10.1002/qj.828, 2011. 21458

Desroziers, G., Berre, L., Chapnik, B., and Poli, P.: Diagnosis of observation, background and analysis-error statistics in observation space, Q. J. Roy. Meteor. Soc., 131, 3385–3396, doi:10.1256/qj.05.108, 2005. 21466

Doughty, D. C., Thompson, A. M., Schoeberl, M. R., Stajner, I., Wargan, K., and Hui, W. C. J.: An intercomparison of tropospheric ozone retrievals derived from two Aura instruments and measurements in western North America in 2006, J. Geophys. Res.-Atmos., 116, D06303, doi:10.1029/2010JD014703, 2011. 21458

ACPD
13, 21455–21505, 2013

Dufour, A., Amodei, M., Ancellet, G., and Peuch, V.-H.: Observed and modelled chemical weather during ESCOMPTE, Atmos. Res., 74, 161–189, doi:10.1016/j.atmosres.2004.04.013, 2005. 21464

Dufour, G., Eremenko, M., Griesfeller, A., Barret, B., LeFlochmoën, E., Clerbaux, C., Hadji-Lazaro, J., Coheur, P.-F., and Hurtmans, D.: Validation of three different scientific ozone products retrieved from IASI spectra using ozonesondes, Atmos. Meas. Tech., 5, 611–630, doi:10.5194/amt-5-611-2012, 2012. 21458, 21461, 21467

El Amraoui, L., Peuch, V.-H., Ricaud, P., Massart, S., Semane, N., Teyssèdre, H., Cariolle, D., and Karcher, F.: Ozone loss in the 2002–2003 Arctic vortex deduced from the assimilation of Odin/SMR O_3 and N_2O measurements: N_2O as a dynamical tracer, Q. J. Roy. Meteor. Soc., 134, 217–228, doi:10.1002/qj.191, 2008a. 21466

El Amraoui, L., Semane, N., Peuch, V.-H., and Santee, M. L.: Investigation of dynamical processes in the polar stratospheric vortex during the unusually cold winter 2004/2005, Geophys. Res. Lett., 35, L03803, doi:10.1029/2007GL031251, 2008b. 21466

El Amraoui, L., Attié, J.-L., Semane, N., Claeyman, M., Peuch, V.-H., Warner, J., Ricaud, P., Cammas, J.-P., Piacentini, A., Josse, B., Cariolle, D., Massart, S., and Bencherif, H.: Midlatitude stratosphere – troposphere exchange as diagnosed by MLS O_3 and MOPITT CO assimilated fields, Atmos. Chem. Phys., 10, 2175–2194, doi:10.5194/acp-10-2175-2010, 2010. 21461, 21466, 21478

Eremenko, M., Dufour, G., Foret, G., Keim, C., Orphal, J., Beekmann, M., Bergametti, G., and Flaud, J. M.: Tropospheric ozone distributions over Europe during the heat wave in July 2007 observed from infrared nadir spectra recorded by IASI, Geophys. Res. Lett., 35, L18805, doi:10.1029/2008GL034803, 2008. 21458

Eskes, H. J. and Boersma, K. F.: Averaging kernels for DOAS total-column satellite retrievals, Atmos. Chem. Phys., 3, 1285–1291, doi:10.5194/acp-3-1285-2003, 2003. 21458

Fioletov, V. E., Bodeker, G. E., Miller, A. J., McPeters, R. D., and Stolarski, R.: Global and zonal total ozone variations estimated from ground-based and satellite measurements: 1964–2000, J. Geophys. Res.-Atmos., 107, 4647, doi:10.1029/2001JD001350, 2002. 21457

Fisher, M. and Andersson, E.: Developments in 4D-Var and Kalman filtering, in: Technical Memorandum Research Departement, ECMWF, Reading, UK, 2001. 21466

Froidevaux, L., Jiang, Y. B., Lambert, A., Livesey, N. J., Read, W. G., Waters, J. W., Browell, E. V., Hair, J. W., Avery, M. A., McGee, T. J., Twigg, L. W., Sumnicht, G. K., Jucks, K. W., Margitan, J. J., Sen, B., Stachnik, R. A., Toon, G. C., Bernath, P. F., Boone, C. D.,

ACPD
13, 21455–21505, 2013

Walker, K. A., Filipiak, M. J., Harwood, R. S., Fuller, R. A., Manney, G. L., Schwartz, M. J., Daffer, W. H., Drouin, B. J., Cofield, R. E., Cuddy, D. T., Jarnot, R. F., Knosp, B. W., Perun, V. S., Snyder, W. V., Stek, P. C., Thurstans, R. P., and Wagner, P. A.: Validation of Aura Microwave Limb Sounder stratospheric ozone measurements, J. Geophys. Res., 113, D15S20, doi:10.1029/2007JD008771, 2008. 21460, 21461, 21470, 21476

Geer, A. J., Lahoz, W. A., Bekki, S., Bormann, N., Errera, Q., Eskes, H. J., Fonteyn, D., Jackson, D. R., Juckes, M. N., Massart, S., Peuch, V.-H., Rharmili, S., and Segers, A.: The ASSET intercomparison of ozone analyses: method and first results, Atmos. Chem. Phys., 6, 5445–5474, doi:10.5194/acp-6-5445-2006, 2006. 21458

Geer, A. J., Lahoz, W. A., Jackson, D. R., Cariolle, D., and McCormack, J. P.: Evaluation of linear ozone photochemistry parametrizations in a stratosphere-troposphere data assimilation system, Atmos. Chem. Phys., 7, 939–959, doi:10.5194/acp-7-939-2007, 2007. 21458, 21465, 21467

Han, W. and McNally, A. P.: The 4D-Var assimilation of ozone-sensitive infrared radiances measured by IASI, Q. J. Roy. Meteor. Soc., 136, 2025–2037, doi:10.1002/qj.708, 2010. 21459

Hegarty, J., Mao, H., and Talbot, R.: Winter- and summertime continental influences on tropospheric O_3 and CO observed by TES over the western North Atlantic Ocean, Atmos. Chem. Phys., 10, 3723–3741, doi:10.5194/acp-10-3723-2010, 2010. 21458

Inness, A., Baier, F., Benedetti, A., Bouarar, I., Chabrillat, S., Clark, H., Clerbaux, C., Coheur, P., Engelen, R. J., Errera, Q., Flemming, J., George, M., Granier, C., Hadji-Lazaro, J., Huijnen, V., Hurtmans, D., Jones, L., Kaiser, J. W., Kapsomenakis, J., Lefever, K., Leitão, J., Razinger, M., Richter, A., Schultz, M. G., Simmons, A. J., Suttie, M., Stein, O., Thépaut, J.-N., Thouret, V., Vrekoussis, M., Zerefos, C., and the MACC team: The MACC reanalysis: an 8 yr data set of atmospheric composition, Atmos. Chem. Phys., 13, 4073–4109, doi:10.5194/acp-13-4073-2013, 2013. 21458

Jackson, D. R.: Assimilation of EOS MLS ozone observations in the Met Office data-assimilation system, Q. J. Roy. Meteor. Soc., 133, 1771–1788, doi:10.1002/qj.140, 2007. 21458, 21470, 21478

Jackson, D. R. and Orsolini, Y. J.: Estimation of Arctic ozone loss in winter 2004/05 based on assimilation of EOS MLS and SBUV/2 observations, 134, 1833–1841, doi:10.1002/qj.316, 2008. 21461

Jaffe, D. and Ray, J.: Increase in surface ozone at rural sites in the western US, Atmos. Environ., 41, 5452–5463, doi:10.1016/j.atmosenv.2007.02.034, 2007. 21457

ACPD
13, 21455–21505, 2013

Jaumouillé, E., Massart, S., Piacentini, A., Cariolle, D., and Peuch, V.-H.: Impact of a time-dependent background error covariance matrix on air quality analysis, Geosci. Model Dev., 5, 1075–1090, doi:10.5194/gmd-5-1075-2012, 2012. 21466

Josse, B., Simon, P., and Peuch, V.: Radon global simulations with the multiscale chemistry and transport model MOCAGE, Tellus B, 56, doi:10.1111/j.1600-0889.2004.00112.x, 2004. 21464

Kar, J., Fishman, J., Creilson, J. K., Richter, A., Ziemke, J., and Chandra, S.: Are there urban signatures in the tropospheric ozone column products derived from satellite measurements?, Atmos. Chem. Phys., 10, 5213–5222, doi:10.5194/acp-10-5213-2010, 2010. 21457

Komhyr, W. D., Barnes, R. A., Brothers, G. B., Lathrop, J. A., and Opperman, D. P.: Electrochemical concentration cell ozonesonde performance evaluation during STOIC 1989, J. Geophys. Res.-Atmos., 100, 9231–9244, doi:10.1029/94JD02175, 1995. 21457, 21462

Lahoz, W. A., Errera, Q., Swinbank, R., and Fonteyn, D.: Data assimilation of stratospheric constituents: a review, Atmos. Chem. Phys., 7, 5745–5773, doi:10.5194/acp-7-5745-2007, 2007a. 21465

Lahoz, W. A., Geer, A. J., Bekki, S., Bormann, N., Ceccherini, S., Elbern, H., Errera, Q., Eskes, H. J., Fonteyn, D., Jackson, D. R., Khattatov, B., Marchand, M., Massart, S., Peuch, V.-H., Rharmili, S., Ridolfi, M., Segers, A., Talagrand, O., Thornton, H. E., Vik, A. F., and von Clarmann, T.: The Assimilation of Envisat data (ASSET) project, Atmos. Chem. Phys., 7, 1773–1796, doi:10.5194/acp-7-1773-2007, 2007b. 21458

Lamarque, J.-F., Khattatov, B. V., and Gille, J. C.: Constraining tropospheric ozone column through data assimilation, J. Geophys. Res., 107, 4651, doi:10.1029/2001JD001249, 2002. 21478

Levelt, P. F., Oord, G. H. J. V. D., Dobber, M. R., Mälkki, A., Visser, H., Vries, J. D., Stammes, P., Lundell, J. O. V., and Saari, H.: The Ozone Monitoring Instrument, IEEE T. Geosci. Remote, 44, 1093–1101, doi:10.1109/TGRS.2006.872333, 2006. 21463

Livesey, N. J., Filipiak, M. J., Froidevaux, L., Read, W. G., Lambert, A., Santee, M. L., Jiang, J. H., Pumphrey, H. C., Waters, J. W., Cofield, R. E., Cuddy, D. T., Daffer, W. H., Drouin, B. J., Fuller, R. A., Jarnot, R. F., Jiang, Y. B., Knosp, B. W., Li, Q. B., Perun, V. S., Schwartz, M. J., Snyder, W. V., Stek, P. C., Thurstans, R. P., Wagner, P. A., Avery, M., Browell, E. V., Cammas, J.-P., Christensen, L. E., Diskin, G. S., Gao, R.-S., Jost, H.-J., Loewenstein, M., Lopez, J. D., Nedelec, P., Osterman, G. B., Sachse, G. W., and Webster, C. R.: Validation of Aura Microwave Limb Sounder O_3 and CO observations in the upper troposphere

ACPD
13, 21455–21505, 2013

and lower stratosphere, J. Geophys. Res., 113, D15S02, doi:10.1029/2007JD008805, 2008. 21460

Ma, J. and van Aardenne, J. A.: Impact of different emission inventories on simulated tropospheric ozone over China: a regional chemical transport model evaluation, Atmos. Chem. Phys., 4, 877–887, doi:10.5194/acp-4-877-2004, 2004. 21459

Marenco, A., Thouret, V., Nédélec, P., Smit, H., Helten, M., Kley, D., Karcher, F., Simon, P., Law, K., Pyle, J., Poschmann, G., Rainer, V. W., Hume, C., and Cook, T.: Measurement of ozone and water vapor by Airbus in-service aircraft: the MOZAIC airborne program, an overview, J. Geophys. Res.-Atmos., 103, 25631–25642, doi:10.1029/98JD00977, 1998. 21463

Massart, S., Piacentini, A., Cariolle, D., El Amraoui, L., and Semane, N.: Assessment of the quality of the ozone measurements from the Odin/SMR instrument using data assimilation, Can. J. Phys., 85, 1209–1223, doi:10.1139/p07-124, 2007. 21466

Massart, S., Clerbaux, C., Cariolle, D., Piacentini, A., Turquety, S., and Hadji-Lazaro, J.: First steps towards the assimilation of IASI ozone data into the MOCAGE-PALM system, Atmos. Chem. Phys., 9, 5073–5091, doi:10.5194/acp-9-5073-2009, 2009. 21459, 21460, 21461, 21466, 21467, 21472

Massart, S., Pajot, B., Piacentini, A., and Pannekoucke, O.: On the merits of using a 3D-FGAT assimilation scheme with an outer loop for atmospheric situations governed by transport, Mon. Weather Rev., 138, 4509–4522, doi:10.1175/2010MWR3237.1, 2010. 21466

Massart, S., Piacentini, A., and Pannekoucke, O.: Importance of using ensemble estimated background error covariances for the quality of atmospheric ozone analyses, Q. J. Roy. Meteor. Soc., 138, 889–905, doi:10.1002/qj.971, 2012. 21459, 21460, 21461, 21466, 21468, 21469, 21470, 21475, 21478, 21491

Miyazaki, K., Eskes, H. J., Sudo, K., Takigawa, M., van Weele, M., and Boersma, K. F.: Simultaneous assimilation of satellite NO_2, O_3, CO, and HNO_3 data for the analysis of tropospheric chemical composition and emissions, Atmos. Chem. Phys., 12, 9545–9579, doi:10.5194/acp-12-9545-2012, 2012. 21459

Oltmans, S. J., Lefohn, A. S., Harris, J. M., Galbally, I., Scheel, H. E., Bodeker, G., Brunke, E., Claude, H., Tarasick, D., Johnson, B. J., Simmonds, P., Shadwick, D., Anlauf, K., Hayden, K., Schmidlin, F., Fujimoto, T., Akagi, K., Meyer, C., Nichol, S., Davies, J., Redondas, A., and Cuevas, E.: Long-term changes in tropospheric ozone, Atmos. Environ., 40, 3156–3173, doi:10.1016/j.atmosenv.2006.01.029, 2006. 21464

ACPD
13, 21455–21505, 2013

Pannekoucke, O. and Massart, S.: Estimation of the local diffusion tensor and normalization for heterogeneous correlation modelling using a diffusion equation, Q. J. Roy. Meteor. Soc., 14, 1–14, doi:10.1002/qj.288, 2008. 21466

Parrington, M., Jones, D. B. A., Bowman, K. W., Thompson, A. M., Tarasick, D. W., Merrill, J., Oltmans, S. J., Leblanc, T., Witte, J. C., and Millet, D. B.: Impact of the assimilation of ozone from the Tropospheric Emission Spectrometer on surface ozone across North America, Geophys. Res. Lett., 36, L04802, doi:10.1029/2008GL036935, 2009. 21458

Paul, J., Fortuin, F., and Kelder, H.: An ozone climatology based on ozonesonde and satellite measurements, J. Geophys. Res.-Atmos., 103, 31709–31734, doi:10.1029/1998JD200008, 1998. 21468

Peuch, V.-H., Amodei, M., Barthet, T., Cathala, M. L., Michou, M., and Simon, P.: MOCAGE, MOdèle de Chimie Atmosphérique à Grande Echelle, in: Proceedings of Météo France: Workshop on Atmospheric Modelling, Toulouse, France, 33–36, 1999. 21464

Remer, L. A., Kleidman, R. G., Levy, R. C., Kaufman, Y. J., Tanré, D., Mattoo, S., Martins, J. V., Ichoku, C., Koren, I., Yu, H., and Holben, B. N.: Global aerosol climatology from the MODIS satellite sensors, J. Geophys. Res., 113, 1–18, doi:10.1029/2007JD009661, 2008. 21471

Solomon, S., Qin, D., Manning, M., Chen, Z., Marquis, M., Averyt, K., Tignor, M., and Miller, H. L.: Contribution of Working Group I to the Fourth Assessment Report of the Intergovernmental Panel on Climate Change, Cambridge University Press, NY, 446 pp., 2007. 21457

Stajner, I., Wargan, K., Pawson, S., Hayashi, H., Chang, L.-P., Hudman, R. C., Froidevaux, L., Livesey, N., Levelt, P. F., Thompson, A. M., Tarasick, D. W., Stübi, R., Andersen, S. B., Yela, M., König-Langlo, G., Schmidlin, F. J., and Witte, J. C.: Assimilated ozone from EOS-Aura: evaluation of the tropopause region and tropospheric columns, J. Geophys. Res., 113, D16S32, doi:10.1029/2007JD008863, 2008. 21461, 21470, 21478

Stohl, A., Bonasoni, P., Cristofanelli, P., Collins, W., Feichter, J., Frank, A., Forster, C., Gerasopoulos, E., Gäggeler, H., James, P., Kentarchos, T., Kromp-Kolb, H., Krüger, B., Land, C., Meloen, J., Papayannis, A., Priller, A., Seibert, P., Sprenger, M., Roelofs, G. J., Scheel, H. E., Schnabel, C., Siegmund, P., Tobler, L., Trickl, T., Wernli, H., Wirth, V., Zanis, P., and Zerefos, C.: Stratosphere-troposphere exchange: a review, and what we have learned from STACCATO, J. Geophys. Res.-Atmos., 108, 8516, doi:10.1029/2002JD002490, 2003. 21457

ACPD
13, 21455–21505, 2013

Tang, Q. and Prather, M. J.: Five blind men and the elephant: what can the NASA Aura ozone measurements tell us about stratosphere-troposphere exchange?, Atmos. Chem. Phys., 12, 2357–2380, doi:10.5194/acp-12-2357-2012, 2012. 21458

Tanimoto, H.: Increase in springtime tropospheric ozone at a mountainous site in Japan for the period 1998–2006, Atmos. Environ., 43, 1358–1363, 2009. 21457

Teyssèdre, H., Michou, M., Clark, H. L., Josse, B., Karcher, F., Olivié, D., Peuch, V.-H., Saint-Martin, D., Cariolle, D., Attié, J.-L., Nédélec, P., Ricaud, P., Thouret, V., van der A, R. J., Volz-Thomas, A., and Chéroux, F.: A new tropospheric and stratospheric Chemistry and Transport Model MOCAGE-Climat for multi-year studies: evaluation of the present-day climatology and sensitivity to surface processes, Atmos. Chem. Phys., 7, 5815–5860, doi:10.5194/acp-7-5815-2007, 2007. 21459, 21464

Thompson, A. M., Witte, J. C., McPeters, R. D., Oltmans, S. J., Schmidlin, F. J., Logan, J. A., Fujiwara, M., Kirchhoff, V. W. J. H., Posny, F., Coetzee, G. J. R., Hoegger, B., Kawakami, S., Ogawa, T., Johnson, B. J., Vömel, H., and Labow, G.: Southern Hemisphere Additional Ozonesondes (SHADOZ) 1998 2000 tropical ozone climatology 1. Comparison with Total Ozone Mapping Spectrometer (TOMS) and ground-based measurements, J. Geophys. Res.-Atmos., 108, 8238, doi:10.1029/2001JD000967, 2003. 21462

van der A, R. J., Allaart, M. A. F., and Eskes, H. J.: Multi sensor reanalysis of total ozone, Atmos. Chem. Phys., 10, 11277–11294, doi:10.5194/acp-10-11277-2010, 2010. 21458

van der Werf, G. R., Randerson, J. T., Giglio, L., Collatz, G. J., Kasibhatla, P. S., and Arellano Jr., A. F.: Interannual variability in global biomass burning emissions from 1997 to 2004, Atmos. Chem. Phys., 6, 3423–3441, doi:10.5194/acp-6-3423-2006, 2006. 21471

Veefkind, J. P., de Haan, J. F., Brinksma, E. J., Kroon, M., and Levelt, P. F.: Total ozone from the ozone monitoring instrument (OMI) using the DOAS technique, IEEE T. Geosci. Remote, 44, 1239–1244, doi:10.1109/TGRS.2006.871204, 2006. 21463

Waters, J. W., Froidevaux, L., Harwood, R. S., Jarnot, R. F., Pickett, H. M., Read, W. G., Siegel, P. H., Cofield, R. E., Filipiak, M. J., Flower, D. A., Holden, J. R., Lau, G. K., Livesey, N. J., Manney, G. L., Pumphrey, H. C., Santee, M. L., Wu, D. L., Cuddy, D. T., Lay, R. R., Loo, M. S., Perun, V. S., Schwartz, M. J., Stek, P. C., Thurstans, R. P., Boyles, M. A., Chandra, K. M., Chave, M. C., Chen, G.-S., Chudasama, B. V., Dodge, R., Fuller, R. A., Girard, M. A., Jiang, J. H., Jiang, Y., Knosp, B. W., LaBelle, R. C., Lam, J. C., Lee, K. A., Miller, D., Oswald, J. E., Patel, N. C., Pukala, D. M., Quintero, O., Scaff, D. M., Van Snyder, W., Tope, M. C., Wagner, P. A., and Walch, M. J.: The Earth observing sys-

ACPD
13, 21455–21505, 2013

tem microwave limb sounder (EOS MLS) on the aura Satellite, IEEE T. Geosci. Remote, 44, 1075–1092, doi:10.1109/TGRS.2006.873771, 2006. 21460
Weaver, A. and Courtier, P.: Correlation modelling on the sphere using a generalized diffusion equation, Q. J. Roy. Meteor. Soc., 127, 1815–1846, 2001. 21466
Yang, Q., Cunnold, D. M., Choi, Y., Wang, Y., Nam, J., Wang, H.-J., Froidevaux, L., Thompson, A. M., and Bhartia, P. K.: A study of tropospheric ozone column enhancements over North America using satellite data and a global chemical transport model, J. Geophys. Res., 115, D08302, doi:10.1029/2009JD012616, 2010. 21457
Zhang, L., Jacob, D. J., Boersma, K. F., Jaffe, D. A., Olson, J. R., Bowman, K. W., Worden, J. R., Thompson, A. M., Avery, M. A., Cohen, R. C., Dibb, J. E., Flock, F. M., Fuelberg, H. E., Huey, L. G., McMillan, W. W., Singh, H. B., and Weinheimer, A. J.: Transpacific transport of ozone pollution and the effect of recent Asian emission increases on air quality in North America: an integrated analysis using satellite, aircraft, ozonesonde, and surface observations, Atmos. Chem. Phys., 8, 6117–6136, doi:10.5194/acp-8-6117-2008, 2008. 21457
Zhang, L., Jacob, D. J., Liu, X., Logan, J. A., Chance, K., Eldering, A., and Bojkov, B. R.: Intercomparison methods for satellite measurements of atmospheric composition: application to tropospheric ozone from TES and OMI, Atmos. Chem. Phys., 10, 4725–4739, doi:10.5194/acp-10-4725-2010, 2010. 21458
Ziemke, J. R., Chandra, S., Duncan, B. N., Froidevaux, L., Bhartia, P. K., Levelt, P. F., and Waters, J. W.: Tropospheric ozone determined from Aura OMI and MLS: Evaluation of measurements and comparison with the Global Modeling Initiative's Chemical Transport Model, J. Geophys. Res., 111, D19303, doi:10.1029/2006JD007089, 2006. 21457
Ziemke, J. R., Chandra, S., Duncan, B. N., Schoeberl, M. R., Torres, O., Damon, M. R., and Bhartia, P. K.: Recent biomass burning in the tropics and related changes in tropospheric ozone, Geophys. Res. Lett., 36, L15819, doi:10.1029/2009GL039303, 2009. 21458
Ziemke, J. R., Chandra, S., Labow, G. J., Bhartia, P. K., Froidevaux, L., a nd Witte, J. C.: A global climatology of tropospheric and stratospheric ozone derived from Aura OMI and MLS measurements, Atmos. Chem. Phys., 11, 9237–9251, doi:10.5194/acp-11-9237-2011, 2011. 21457, 21474

ACPD
13, 21455–21505, 2013

Table 1. Description of the model configuration for the assimilation experiments.

Assimilation	Type 4-D-VAR	Description 12 h window
Background Error	Vertically variable (1-D)	Logistic function: 30 % troposphere, 5 % stratosphere
Background Error Zonal Correlation	Horizontally variable (1-D)	Based on ensembles (Massart et al., 2012)
Background Error Meridional Correl.	Constant	300 km
Background Error Vertical Correl.	Constant	1 grid point length scale
IASI observation error	Percentage of measurement	15 %
MLS observation error	From retrieval product	–

ACPD
13, 21455–21505, 2013

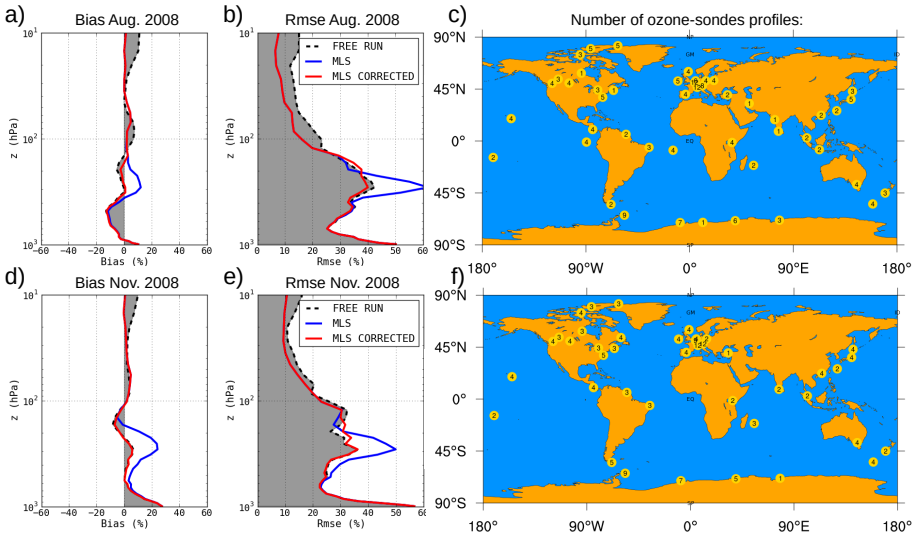

Fig. 1. Validation of model free run (dotted/gray-filled lines) and MLS analyses (blue/red lines) vs. ozone-sondes: **(a)** global bias (model-sondes) normalized with the ozone climatology for August 2008 **(b)** global Root Mean Square Error (RMSE) of model-sondes for August 2008 **(c)** number of ozone-sondes profiles used for the validation **(d)–(f)** same as **(a)–(c)** but for November 2008. Blue lines are obtained by assimilating full MLS profiles whereas for red ones the lowermost profile level (215 hPa) is excluded. Positive/negative values in **(a), (d)** mean that the model overestimates/underestimates the ozone-sondes measurements.

ACPD
13, 21455–21505, 2013

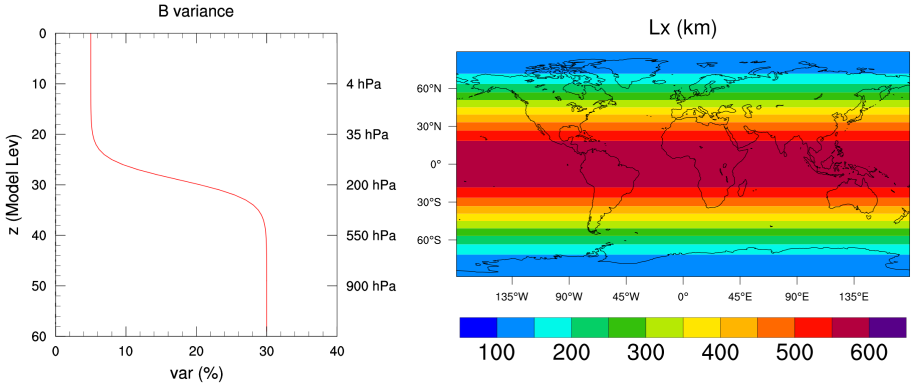

Fig. 2. Main parametrizations of the background covariance matrix (**B**): (left) background error variance in % of the background profile; (right) zonal error correlation length scale (Lx). Blue/purple end colors represent values that fall outside the color scale.

ACPD
13, 21455–21505, 2013

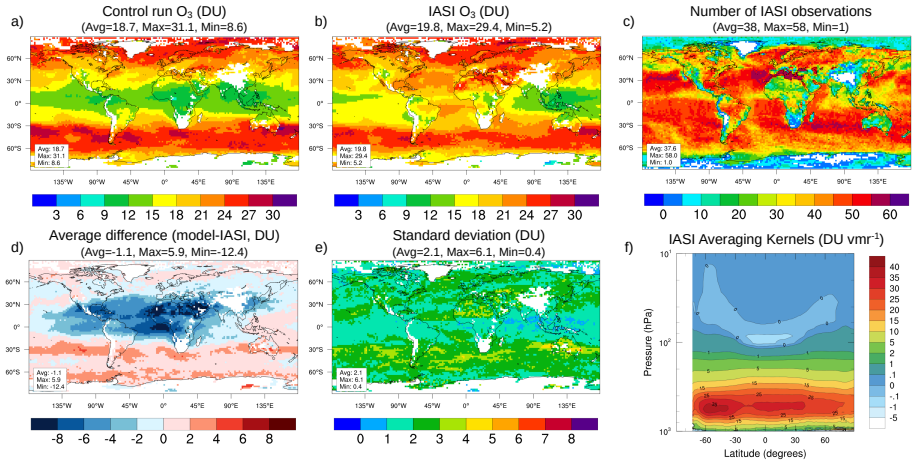

Fig. 3. Average differences between model free run and IASI tropospheric columns (TOC, 1000–225 hPa) for August 2008: **(a)** model free run column weighted by IASI averaging kernels ($AVK \cdot x_{mod}$, where x_{mod} is the model profile) **(b)** IASI equivalent column ($C_{obs} - C_{apr} + AVK \cdot x_{apr}$, where x_{apr} is the IASI a-priori profile and C_{obs},C_{apr} the retrieved and a-priori partial columns) **(c)** number of IASI observations **(d)** bias (model-IASI) **(e)** standard deviation of model-IASI **(f)** IASI averaging kernels (zonal average in DU vmr^{-1}). All IASI values are reduced by 10 % to account for retrieval biases (Sect. 2). Blue/purple/dark-red end colors represent values that fall outside the color scale. White color indicates pixels with a statistically insignificant number of observations ($n < 10$).

ACPD
13, 21455–21505, 2013

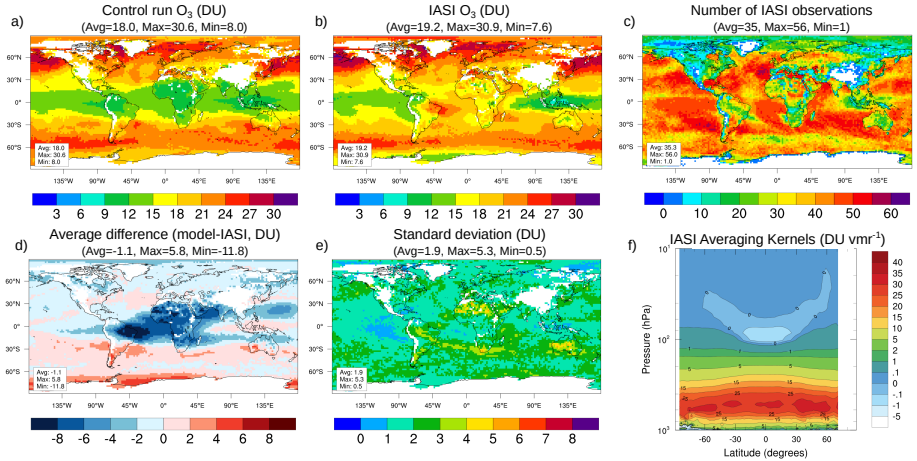

Fig. 4. Average differences between model free run and IASI tropospheric columns (TOC, 1000–225 hPa) for November 2008. Same plots as in Fig. 3.

ACPD
13, 21455–21505, 2013

Combined assimilation of IASI and MLS ozone observations

E. Emili et al.

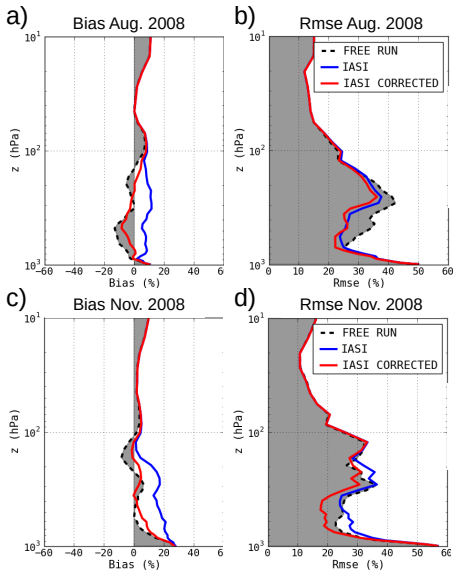

Fig. 5. Validation of model free run and IASI analyses vs. ozone-sondes. Same plots as in Fig. 1 (August 2008 and November 2008 from top to bottom). Red curves are obtained removing 10 % of the IASI ozone values before the assimilation.

ACPD
13, 21455–21505, 2013

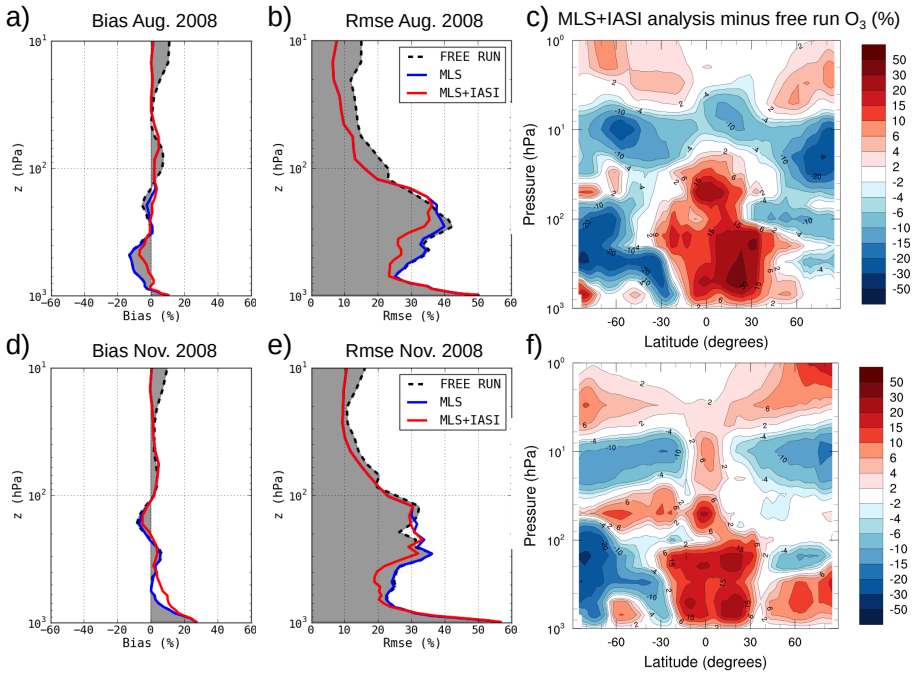

Fig. 6. Validation of model free run, MLS analysis and combined IASI-MLS analysis vs. ozonesondes. **(a), (b), (d), (e)** same plots as in Fig. 1 (August 2008 and November 2008 from top to bottom) **(c), (f)** average zonal difference between model free run and IASI+MLS analysis normalized with climatology. Dark-blue/red end colors represent values that fall outside the color scale.

ACPD
13, 21455–21505, 2013

Combined assimilation of IASI and MLS ozone observations

E. Emili et al.

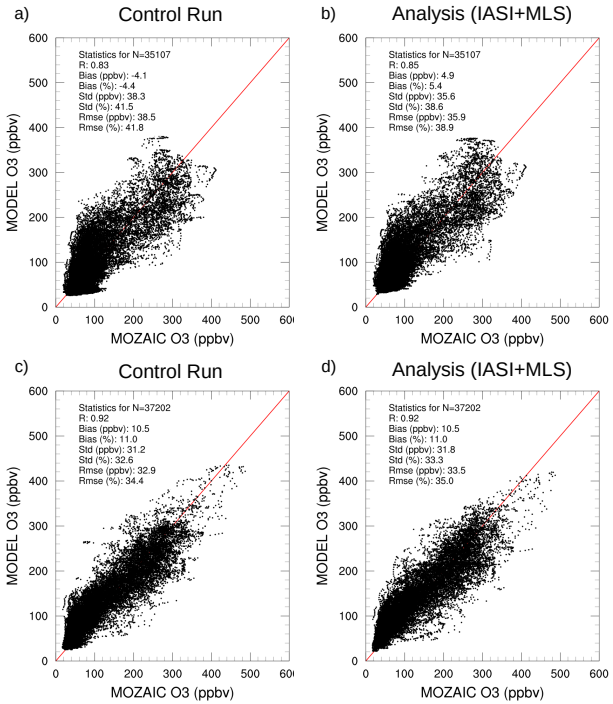

Fig. 7. Validation of model ozone values vs. MOZAIC observations above 400 hPa: **(a)** scatter plot between model free run and MOZAIC values for August 2008 **(b)** scatter plot between IASI+MLS analysis and MOZAIC values for August 2008 **(c), (d)** same as **(a), (b)** but for November 2008. Difference statistics are displayed on each plot in term of number of points (*N*), correlation (*R*), bias in ppbv (model-measurements), relative bias (bias/measurements average), standard deviation in ppbv (std), relative standard deviation (std/measurements average), RMSE in ppbv and relative RMSE (RMSE/measurements average).

ACPD
13, 21455–21505, 2013

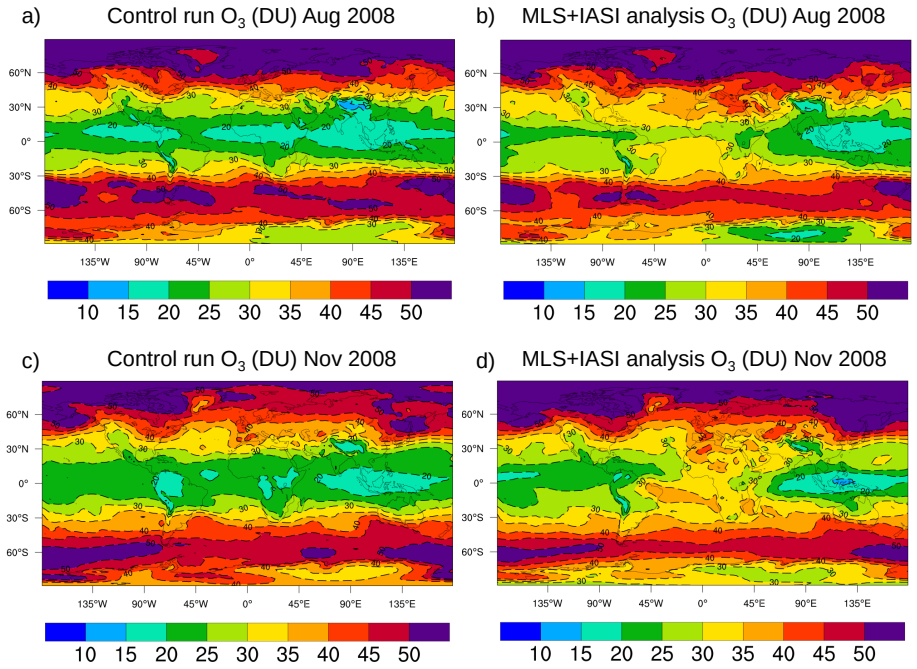

Fig. 8. Ozone tropospheric partial columns (TOC, 225–1000 hPa): **(a)** model free run for August 2008 **(b)** MLS+IASI analysis for August 2008 **(c)** Model free run for November 2008 **(d)** MLS+IASI analysis for November 2008. Blue/purple end colors represent values that fall outside the color scale.

ACPD
13, 21455–21505, 2013

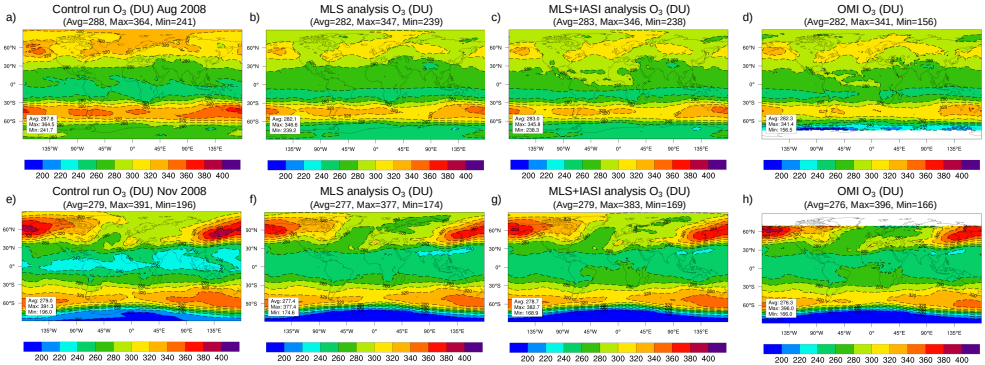

Fig. 9. Validation of model total ozone columns vs. OMI measurements: **(a)** model free run average ozone column for August 2008 **(b)** MLS analysis for August 2008 **(c)** MLS+IASI analysis for August 2008 **(d)** OMI measurements for August 2008 **(e–h)** the same plots but for November 2008. Blue/purple end colors represent values that fall outside the color scale. White color in **(d), (h)** indicates pixels without OMI observations.

ACPD
13, 21455–21505, 2013

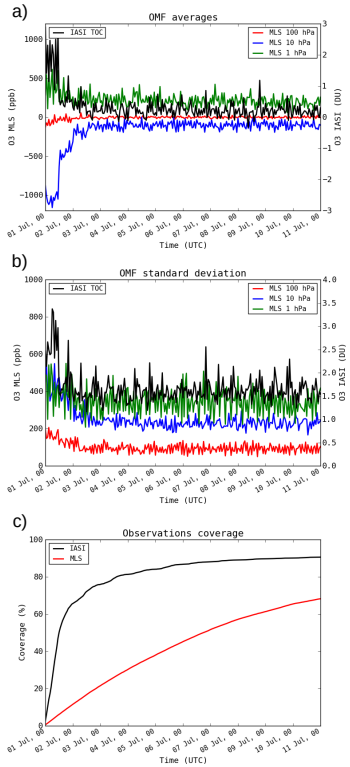

Fig. 10. Observation minus Forecast (OmF) statistics for the first 10 days of the IASI+MLS long analysis (1–10 July 2008). Assimilated observations minus their model equivalent values are averaged globally for each hour. **(a)** OmF average **(b)** OmF standard deviation **(c)** temporal evolution of the observations global coverage (fraction of model horizontal grid pixels visited by the satellite). IASI TOC columns minus their model equivalent (as in Fig. 3) are represented with a black line. MLS observations minus their model equivalent with red (100 hPa level), blue (10 hPa) and green (1 hPa) line.

ACPD
13, 21455–21505, 2013

Combined assimilation of IASI and MLS ozone observations

E. Emili et al.

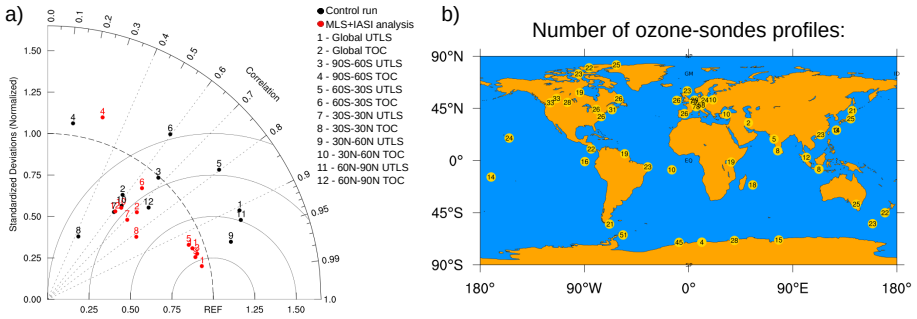

Fig. 11. Global and zonal validation of MLS+IASI analysis partial columns (TOC, UTLS) vs. ozone-sondes for the long analysis run (July-December 2008) **(a)** Taylor diagram (control run in black, analysis in red) **(b)** number of used ozone-sondes profiles.

ACPD
13, 21455–21505, 2013

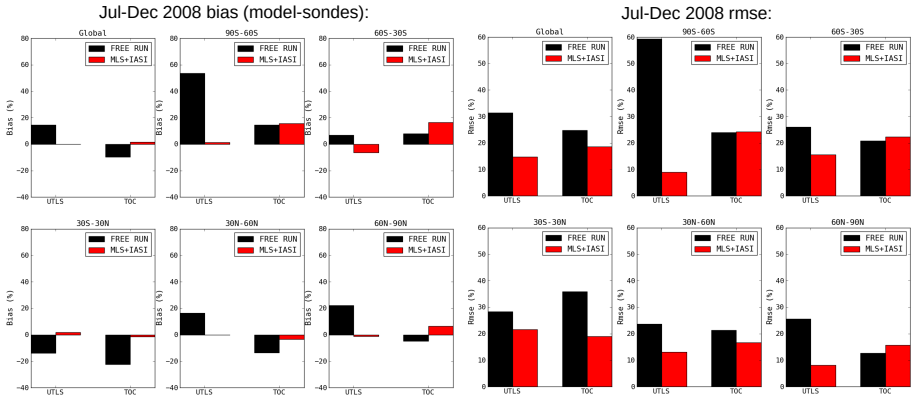

Fig. 12. Global and zonal validation of MLS+IASI analysis partial columns (TOC, UTLS) vs. ozone-sondes for the long analysis run (July–December 2008): left plots: bias (model-sondes) normalized with the climatology (control run in black, analysis in red), right plots: RMSE normalized with the climatology.

ACPD
13, 21455–21505, 2013

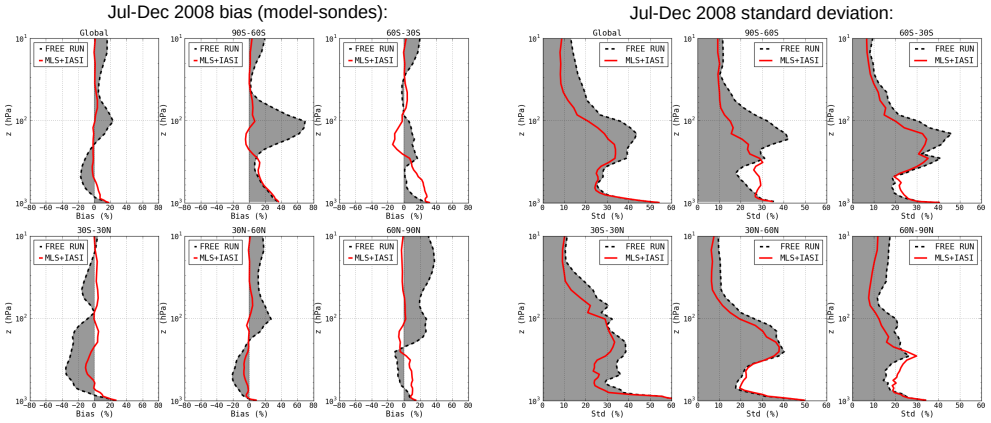

Fig. 13. Global and zonal validation of MLS+IASI analysis vs. ozone-sondes profiles for the long analysis run (July–December 2008): left plots: bias (model-sondes) normalized with the climatology (control run in black, analysis in red), right plots: standard deviation normalized with the climatology.

ACPD
13, 21455–21505, 2013

Combined assimilation of IASI and MLS ozone observations

E. Emili et al.

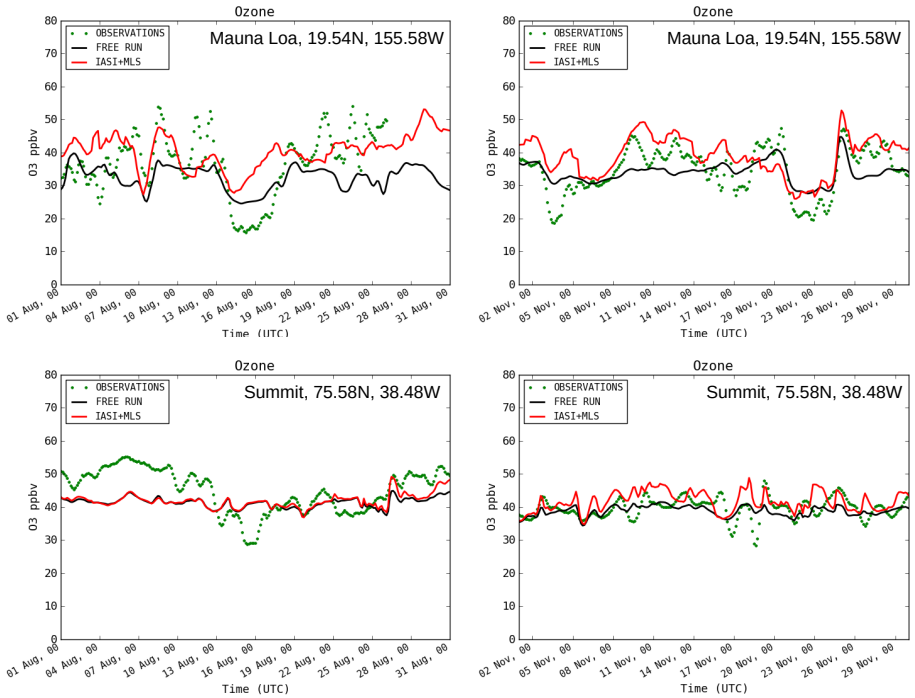

Fig. 14. Time series of hourly measured ozone mixing ratio (green dots) at the sites of Mauna Loa (MLO, 19.54 N, 155.58 W, 3397 m a.s.l., US) and Summit (SUM, 75.58 N, 38.48 W, 3216 m a.s.l., Greenland) in August/November 2008 and correspondent model predictions: control run (black line), IASI+MLS analysis (red line).

ACPD
13, 21455–21505, 2013

Combined assimilation of IASI and MLS ozone observations

E. Emili et al.